IOP Publishing Superconductor Science and Technology
Supercond. Sci. Technol. **33** (2020) 085010 (22pp) https://doi.org/10.1088/1361-6668/ab9ad1

CORC® wires containing integrated optical fibers for temperature and strain monitoring and voltage wires for reliable quench detection

D C van der Laan[1,2,4], J D Weiss[1,2], F Scurti[3] and J Schwartz[3]

[1] Advanced Conductor Technologies, Boulder, CO 80301, United States of America
[2] University of Colorado, Boulder, CO 80309, United States of America
[3] Department of Engineering Science and Mechanics, Pennsylvania State University, University Park, PA 16802, United States of America

E-mail: danko@advancedconductor.com

Received 23 February 2020, revised 21 May 2020
Accepted for publication 9 June 2020
Published 7 July 2020

Abstract

Safe operation of large superconducting magnets wound from high-temperature superconductors (HTS) requires reliable detection of the onset of a quench. A novel method to integrate optical fibers and voltage wires within the core of multi-tape HTS CORC® wires has been developed that allows real time monitoring of local changes in strain, temperature and of the superconducting state of the magnet windings. The ability to detect highly localized changes in temperature with Rayleigh scattering in the embedded optical fibers provides invaluable information about local heating at hot spots from which a quench may originate. Integrated voltage contacts allow accurate voltage measurements in long CORC® wires without being affected by high current ramp rates or electromagnetic interference. They also allow detection of inductively driven redistribution of current between tapes in CORC® wires that may occur at high current ramp rates. Continuous monitoring of temperature and voltage was used to detect the formation of local hot spots induced by a heater or by operating the CORC® wire above its critical current. The results show that, within the boundary conditions of the experiment and the method by which the optical fibers were integrated into the CORC® wire in this study, the speed and resolution with which hot spots can be detected with optical fibers lagged that of the integrated voltage wires. This study also shows that integrated voltage wires reliably detected the formation of a local hot spot in a 5.1 meter long coiled CORC® wire, down to a hot spot size covering 0.1% of the conductor length and at current ramp rates as high as 2000 A s^{-1}. Voltage measurements thus remain an effective option for quench detection in magnets wound with HTS conductors for which current sharing between tapes allows for operation within the flux flow regime.

Keywords: quench detection, optical fibers, high current ramp rates, CORC® wire

(Some figures may appear in colour only in the online journal)

[4] Author to whom any correspondence should be addressed.

1. Introduction

High-temperature superconductors (HTS) are an enabling technology for the production of high-field superconducting magnets that operate at fields exceeding 20 T and at temperatures far above the boiling point of liquid helium. Such magnets would allow particle accelerators to operate at much higher beam energies, or compact fusion magnets to contain demountable joints, something that is beyond the capabilities of magnets wound from low-temperature superconductors (LTS). Several HTS materials are being developed into practical high-field magnet conductors, including $Bi_2Sr_2CaCu_2O_x$ (Bi-2212) wires [1, 2], $Bi_2Sr_2Ca_2Cu_3O_x$ (Bi-2223) tapes [3, 4] and RE-$Ba_2Cu_3O_{7-\delta}$ (REBCO) coated conductors [5–7], where RE refers to various rare earth elements. One of the key remaining challenges with operating HTS magnets is to detect an incipient magnet quench. The low quench propagation speed in HTS, compared to LTS materials, and the larger temperature margins makes reliable quench detection in long conductors challenging [8–10]. A local hot spot may not be detected in time using conventional quench detection methods such as voltage measurements, resulting in a local burnout of the conductor.

The risk of local burnout is especially high in magnets wound from single insulated conductors that result in a high magnet inductance. The challenge to detect the formation of a local hot spot that may propagate only slowly has resulted in the evaluation of several alternative methods to quench detection in HTS magnets. These methods include, but are not limited to, the use of Rayleigh scattering in optical fibers [11–14], the use of Hall probe arrays [15], and acoustic sensing methods [16, 17]. Although these methods offer various advantages over voltage contact quench detection they are not subject to inductive voltages or electromagnetic interference (EMI), their effectiveness as reliable quench detection method in large magnets still needs to be proven.

Low-inductance magnets that operate at significant current ramp rates require high-current windings that cannot be achieved with a single conductor. A high number of Bi-2212 wires [18, 19], or REBCO coated conductors [20–27] need to be bundled into high-current magnet cables to allow operation at currents exceeding 5 kA in a background field of 20 T. Although current sharing between wires or tapes in these cables allows for relatively stable magnet operation into the flux flow regime [28–32], reliable quench detection remains a requirement for safe operation of such large HTS magnets. An open question for such large magnets is whether reliable quench detection can be based on voltage measurements via the use of multi-tape HTS conductors, or if quench detection depends upon the further development of an alternative method.

This paper describes the results of experiments using high-current CORC® magnet wires targeted for use in low-inductance magnets, where voltage wires and optical fibers are integrated within the central core of the conductor. The instrumentation allows continuous monitoring of the operating state of the CORC® wire. Rayleigh scattering in optical fibers is used to detect heating at the cable terminations and at local hot spots that may develop at currents exceeding the critical current (I_c) of the CORC® wire, or when induced by a local heater. Quench detection with optical fibers is compared to that when using integrated voltage contacts. The potential limits to quench detection using voltage contacts are explored in long CORC® wires, where the hot spot size is varied with respect to the overall conductor length. Integrated voltage wires, in which inductive pickup is minimized, are also used to detect quenches during high current ramp rates and to investigate the effect of the current ramp rate on the current distribution between tapes in long CORC® wires.

2. Experimental

2.1. Integration of voltage wires and optical fibers into CORC® wires

Optical fibers and voltage wires were integrated into CORC® wires by placing them into grooves that were extruded into the 2.6 mm thick copper core. Three grooves of about 0.25 mm in width were extruded along the length of the core, while a twist pitch was introduced by twisting the core after extrusion. The twist pitch is intended to ensure the optical fibers do not break when the CORC® wire is bent, as long as the fibers are able to slide within the groove during bending. Vacuum grease was applied to the grooves before the fibers were inserted to smoothen the surface before tapes were wound onto the core. The grooves became narrower during twisting and the smallest pitch at which the fibers would still fit into the groove was 38 mm (figure 1). The twist pitch of the optical fiber in the groove in combination with the vacuum grease thus ensures the fiber will not accumulate significant stress when the CORC® wire is bent that may cause it to break. On the other hand, the fiber will experience axial strain during magnet operation, which is likely not influenced by the twist pitch or the vacuum grease. The fiber likely follows a similar strain state as the REBCO tapes in the CORC® wire that are also able to slide during bending but will experience the axial strain during magnet operation.

Two optical fibers (fibers #1 and #2) and one insulated voltage wire were wound into grooves of the core. The fibers are single-mode, telecommunication-grade with an outer diameter of 245 μm. A total of eight superconducting tapes were then wound onto the former in four layers to complete a CORC® wire (CORC®-O). The tapes from SuperPower Inc. were 2 mm wide and contained a substrate of 30 μm thickness and had copper surround plating with total thickness of 10 μm. The CORC® wire contained tapes with an average I_c at 77 K, self-field of 56 A, resulting in a nominal CORC® wire I_c of 448 A. The CORC® wire, 0.24 m in length between terminations, was terminated using two copper tubes of 10 cm in length in which each tape layer of the CORC® wire was tapered [26]. Figure 2(a) shows the fibers and voltage contact extending beyond the former. The tubes were filled with 100-In solder to make electrical contact to the tapes, while the optical fibers and voltage contact extended from the former, through the solder of the terminations (figure 2(b)).

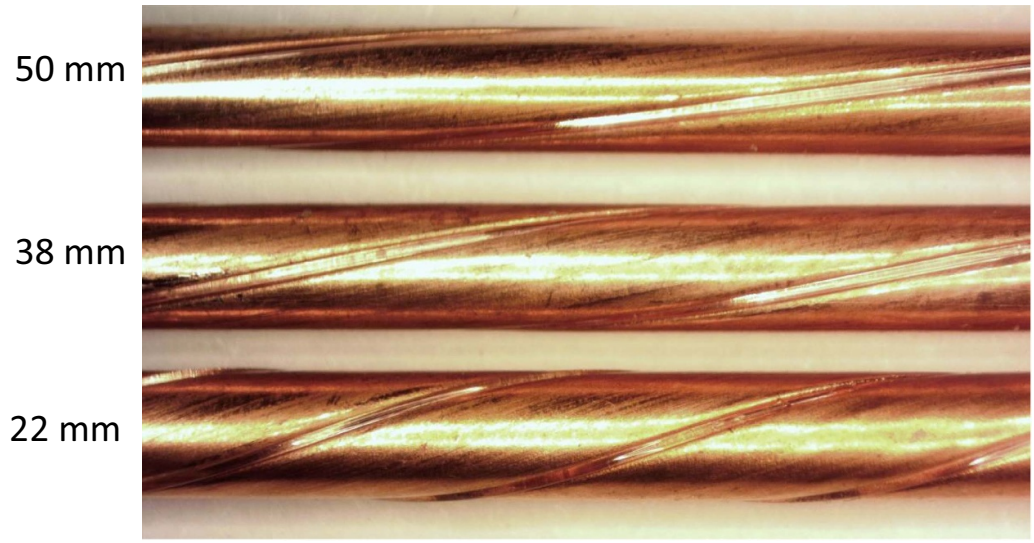

Figure 1. Copper core with optical fibers embedded into its grooves. The formers were twisted at different twist pitch lengths. The twist pitch length is indicated in the figure.

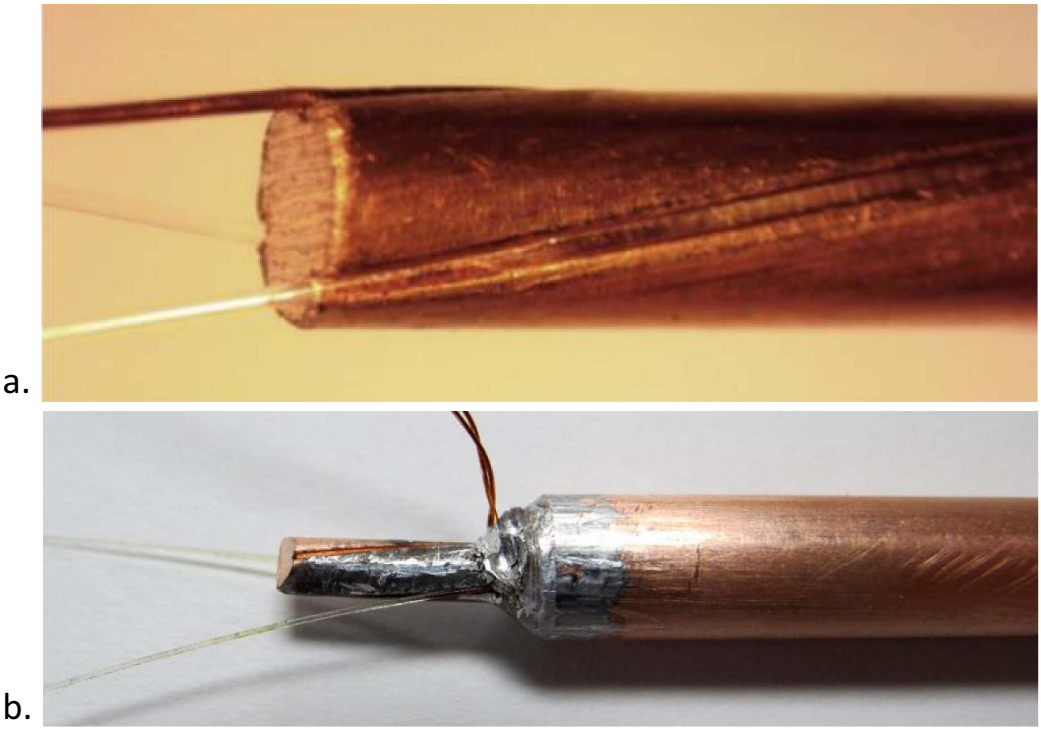

Figure 2. (a) Two optical fibers and one insulated voltage contact extending from the grooves in the copper core, and (b) extending from the solder-filled terminations.

The CORC® wire contained two voltage wires (V1 and V2) that were co-wound around the outside of the CORC® wire and one integrated voltage wire (V3) (see figure 3(a)). Voltage contacts V1 and V2 were connected between the superconducting layers of the CORC® wire and the copper terminations, about a third of the way into the termination when measured from the side where the CORC® wire exits. A NiCr heater wire, with total resistance of 4.7 Ω, was wound over a distance of 5 mm in the center of the CORC® wire to allow formation of a local hot spot.

2.2. Current injection into CORC® wire terminals

Current injection into the copper terminals of the CORC® wires was performed by clamping aluminum or copper adapters onto the terminals. Small aluminum adapters that cover about 50% of the terminal length were used to study the thermal implications of localized current injection into the terminals (figure 4(a)), while larger copper adapter shells that cover the entire terminal (figure 4(b)) were used in most experiments. The two copper shells ensure even current injection

Figure 3. Location of the voltage contacts and optical fibers extending from the CORC® wire terminations. Each voltage wire of a voltage wire pair connects to one of the sample terminations. One wire of voltage contact pairs V1 and V2 are co-wound on the outside of the CORC® wire and end near the middle of the termination that's not shown, while one wire of contact pair V3 is located in the grooved former and connects to the furthest end of the termination that not show in the figure. The second voltage wire of each of the pairs is connected to termination visible in the figure.

along the entire length of the termination such that each tapered layer of tapes would experience a comparable contact resistance. Sufficient space between the two copper shells allowed for safe routing of the optical fibers and voltage contacts from the terminations.

2.3. Sample layout during temperature and strain measurements using optical fibers

Several measurements were carried out on sample CORC®-O, containing two optical fibers. The spectral shift of the optical signal, determined using Rayleigh scattering, was measured along the fiber length at a spatial resolution of 0.26 mm. Figure 5 shows an overview of the CORC® wire and the exact location of its terminations along the x-axis, where $x = 0$ and 0.42 m correspond to the locations where the fibers exit the CORC® wire terminals. Figure 5 also shows the case where the small aluminum adapters were used to inject current into the CORC® wire terminations. Either two small adapters (figure 5(a)), or a small aluminum and a large copper adapter were used (figure 5(b)). The overview shows the location along the x-axis that was covered by the small adapters. A third layout, where the two larger copper adapters were used, is not shown.

2.4. CORC® wire construction for quench detection studies with embedded voltage wires

A CORC® wire 5.1 m in length between terminations (sample CORC®-VL), was wound from 8 tapes of 2 mm width, and contained a 2.6 mm thick solid copper former with extruded grooves. The tapes had similar properties as those used to wind sample CORC®-O, although their average I_c was slightly lower at 50 A. The grooves in the former were twisted at a pitch of 38 mm and contained three embedded voltage wires. The CORC® wire was wound into a 0.25 m diameter coil, with turns spaced by 2 cm to reduce the effect of self-field on the conductor (figure 6). The sample contained two voltage contact pairs that were not co-wound with the CORC® wire. One of the voltage contact pair (V1) was soldered within the terminals, about 2/3rd of the way from the termination end, while the other voltage contact pair (V2) was soldered at both termination ends. The sample also contained several embedded voltage wires that were placed in the grooves of the former (V3 and V4) and soldered at the ends of the terminals.

The CORC® wire contained two heaters that were mounted within 0.2 m from one of the terminations. One heater was a 50 mm long heater strip, while the other heater was a NiCr heating wire that was wound over the CORC® wire and covered a length of 5 mm (figure 7). The two heaters of different size allowed the determination of the effect of the hotspot size on the quench detection sensitivity of the voltage wires.

The section of the CORC® wire containing the two heaters was cut off after all tests on the 5.1 m long sample were completed. A new terminal was mounted, forming a shorter sample of 0.47 m in length between the terminals (sample CORC®-VS). Comparing the voltage response of the long, coiled sample to that of the short, straight sample would allow the determination of how the quench detection with voltage contacts would be affected by sample length.

3. Results

3.1. CORC® wire performance

The performance of the CORC® wires containing optical fibers and voltage contacts was tested in liquid nitrogen to confirm the superconducting tapes carry the expected current and that the voltage contacts were intact. Figure 8 shows the electric field versus current (E–I) characteristic measured with voltage contacts V1 and V3 of sample CORC®-O containing two optical fibers and one voltage wire. Figure 9 shows the same for the 5.1 meter long CORC® wire containing three integrated voltage wires (CORC®-VL) after it was wound into a 4.5 turn coil. Both measurements were taken at a current ramp rate of 50 A s^{-1}. The critical current and contact resistance of the terminations was calculated with:

$$V = IR + V_c\left(\frac{I}{I_c}\right)^n + V_0 \tag{1}$$

where R is the contact resistance, V_0 is the inductive voltage offset, n is a fitting parameter known as the n-value, and V_c is the critical voltage based on a contact length (L) and

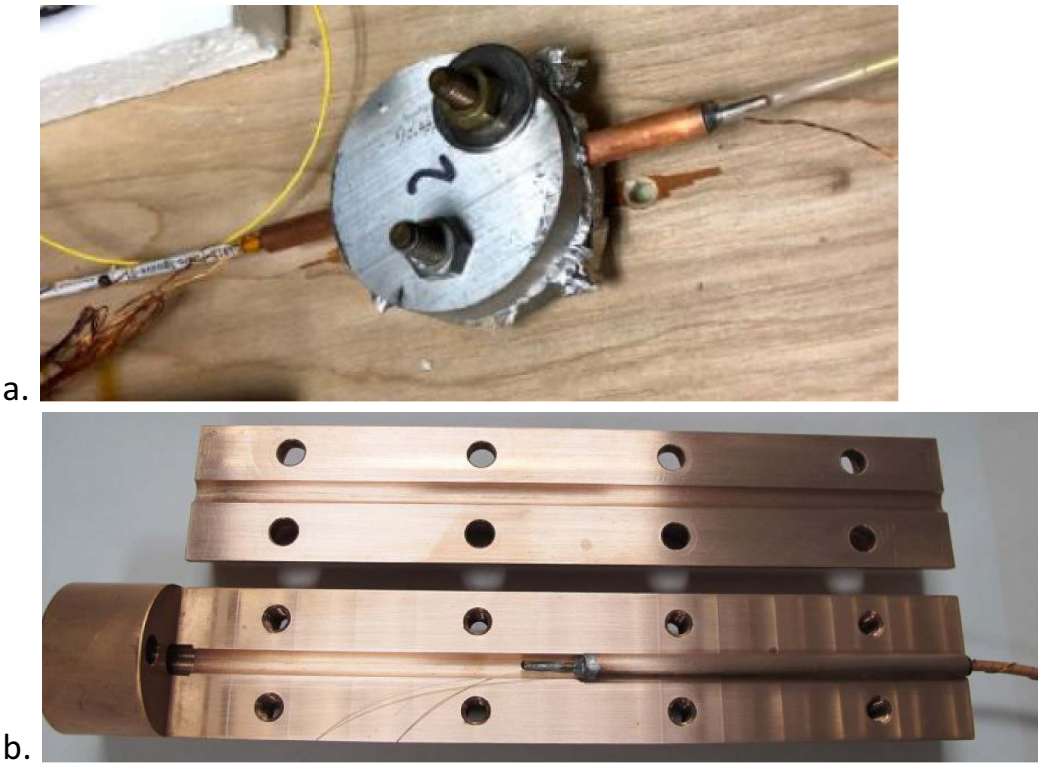

Figure 4. (a) Small aluminum injection adapter covering about 50% of the CORC® wire termination length. (b) CORC® wire termination located in one of the two shells of the larger copper current adapters. The optical fibers and voltage contact were routed through the opening between the two halves.

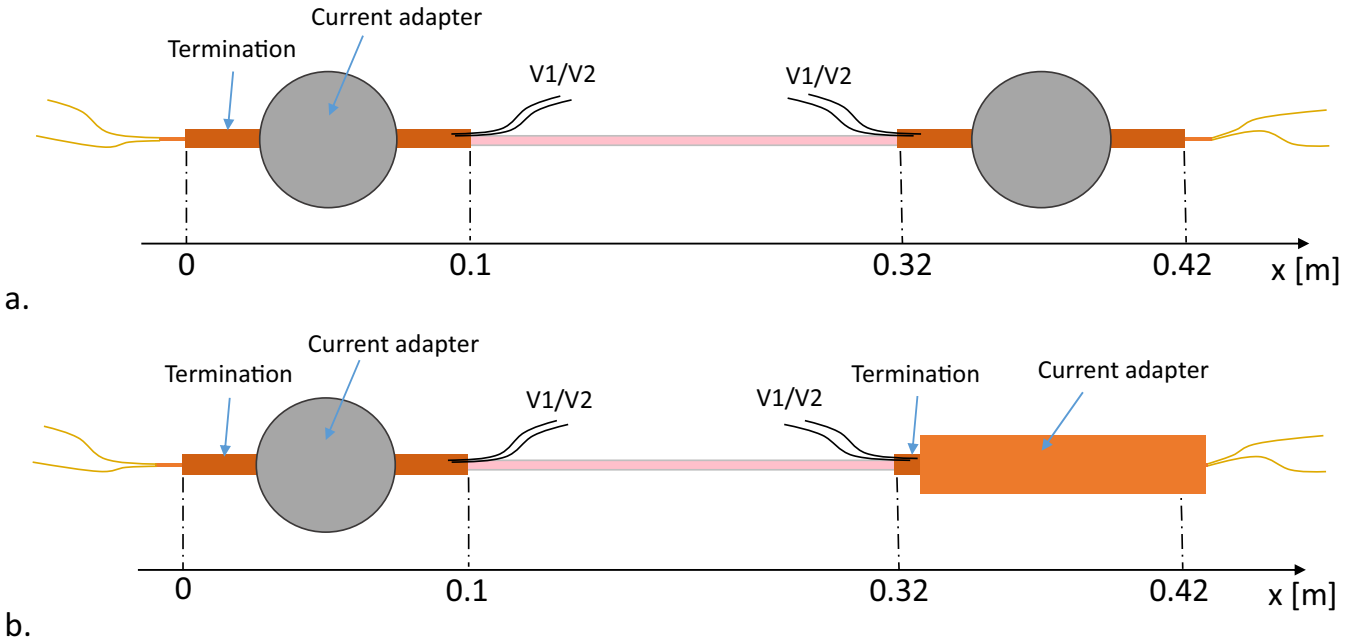

Figure 5. Overview of sample CORC®-O during measurement of temperature and strain change using optical fibers. (a) Current is injected using small aluminum adapters, and (b) using a small aluminum and a large copper adapter.

electric field criterion (E_c) of 1 μV cm^{-1}. The sample performance is listed in table 1, showing that both samples performed as expected, while the integrated voltage wires survived the CORC® wire manufacturing process. The offset voltages measured over the 5.1 m long coiled CORC® wire with the integrated voltage wire (V3) was 0.023 mV, while that measured with the external voltage wires (V1 and V2) was 0.57 mV. The much lower inductive offset voltage shows

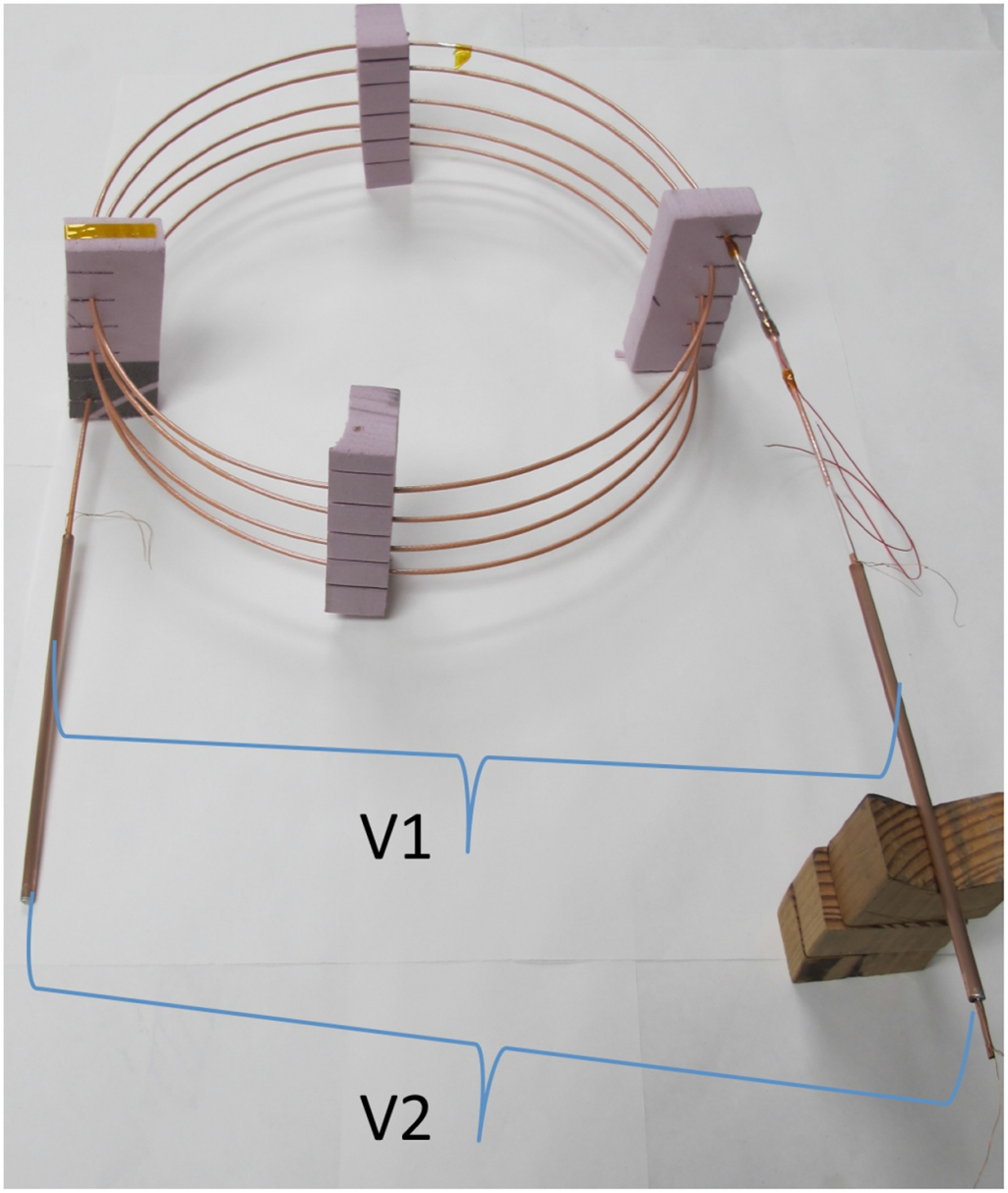

Figure 6. CORC® wire (CORC®-VL) 5.1 m in length containing external (V1 and V2) and integrated voltage contacts.

Figure 7. Heating wire covering 5 mm of the CORC® wire length.

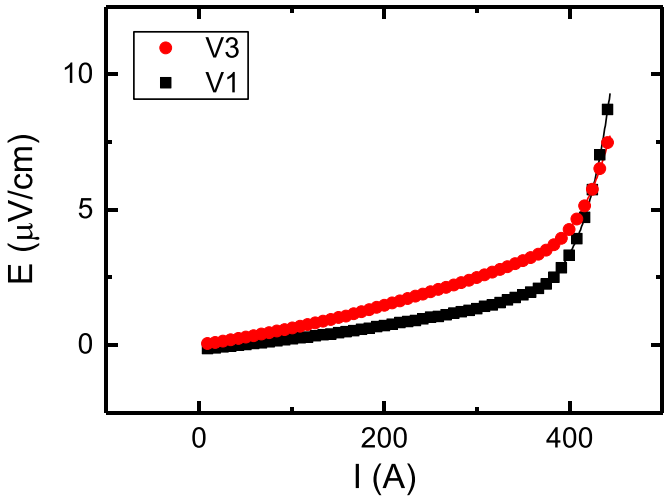

Figure 8. Electric field as a function of current measured at 76 K in liquid nitrogen with external voltage contacts V1 and integrated contacts V3 over the CORC® wire containing optical fibers (sample CORC®-O).

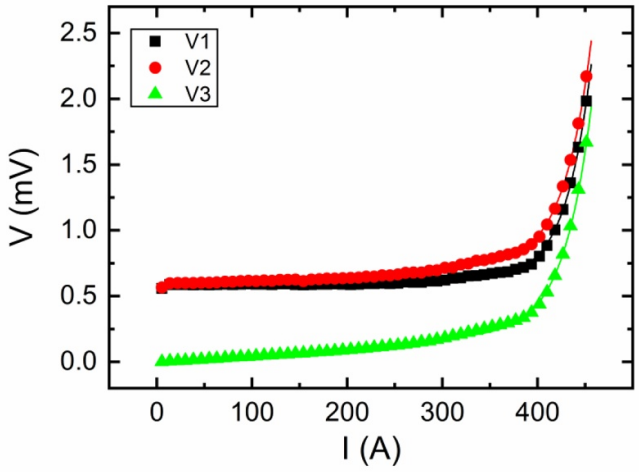

Figure 9. Voltage as a function of current measured at 76 K in liquid nitrogen on the 5.1 meter long CORC® wire (sample CORC®-VL) with the two external voltage contacts (V1 and V2) and one integrated voltage contact (V3).

one benefit of the integrated voltage wires, where inductive voltages are minimized even in a coiled sample.

3.2. Local strain state measured with integrated optical fibers during CORC® wire bending

The ability to bend the CORC® wire containing optical fibers without breaking them is enabled by the twist pitch of the groove in which the fiber is able to slide during bending. To verify this, the CORC® wire was bent at room temperature to diameters ranging from 20 cm to 12 cm. The response of the two optical fibers was first measured when the sample was straight, which provided the measurement baseline. The spectral shift measured in fiber #1 is shown in figure 10 for different bending diameters of the CORC® wire. Figure 11 shows

Table 1. Performance of the CORC® wire samples at 76 K measured with integrated voltage wires.

Sample	CORC® wire length (m)	I_c (A)	n-value (-)	R (nΩ)
CORC®-O	0.26	399	13.3	385
CORC®-VL	5.1	425.9	16	655
CORC®-VS	0.47	405	14	642

the change in local strain state along the length of the fiber that was calculated from the spectral shift using a conversion factor of 1460 GHz/%, similar to what was found in [33]. The presence of friction that would prevent the fiber from sliding freely within the groove during bending would result in a local increase (tension) and decrease (compression) in strain state with a period equal to the twist pitch of the groove (38 mm). Such variations in strain state were indeed measured, but a variation with much longer periodicity in the order of about 0.25 m was also measured.

The change in spectral shift at the much longer periodicity during bending was potentially caused by the change in overall strain state caused by a change in curvature of the fiber. A correction for this baseline shift was made by using a 6th order polynomial fit that described the overall dependence of the change in strain with location, as is shown in figure 12 for the case when the CORC® wire is bent to 15 cm diameter. The change in strain state after subtracting the corrected baseline is also included in the figure and now shows a set of positive and negative peaks with roughly the same absolute value and periodicity of about 40 mm. The polynomial fit was not able to describe the data accurately for the locations of the terminations (x = 0–0.1 and x = 0.32–0.42 m).

Figure 13 shows the change in strain after correction of the baseline signal for each CORC® wire bending diameter. The corrected strain at the locations of both terminations is omitted from the figure for clarity. The figure shows that bending the CORC® wire from straight down to 20 cm diameter added strain of about 0.04% in compression and tension to the optical fiber. The strain increased slightly when the CORC® wire was bent to 18 cm diameter and remained unchanged when the CORC® wire was bent to 12 cm diameter. The peak strain in the fiber was between −0.006% and 0.006% depending on the location along the fiber, with a periodicity of about 40 mm.

The results show that the optical fibers are highly sensitive to a change in the local strain state. Measurement of the change in strain state in CORC® wires due to Lorenz force during operation in high-field magnets would likely be more straightforward. The change in strain state of the fiber would predominantly be caused by hoop stress during magnet energization, while the overall shape of the fiber would remains unchanged.

3.3. Detection of Ohmic heating in CORC® terminations with optical fibers

Measurement of the local change in temperature of sample CORC®-O using the embedded optical fibers was performed

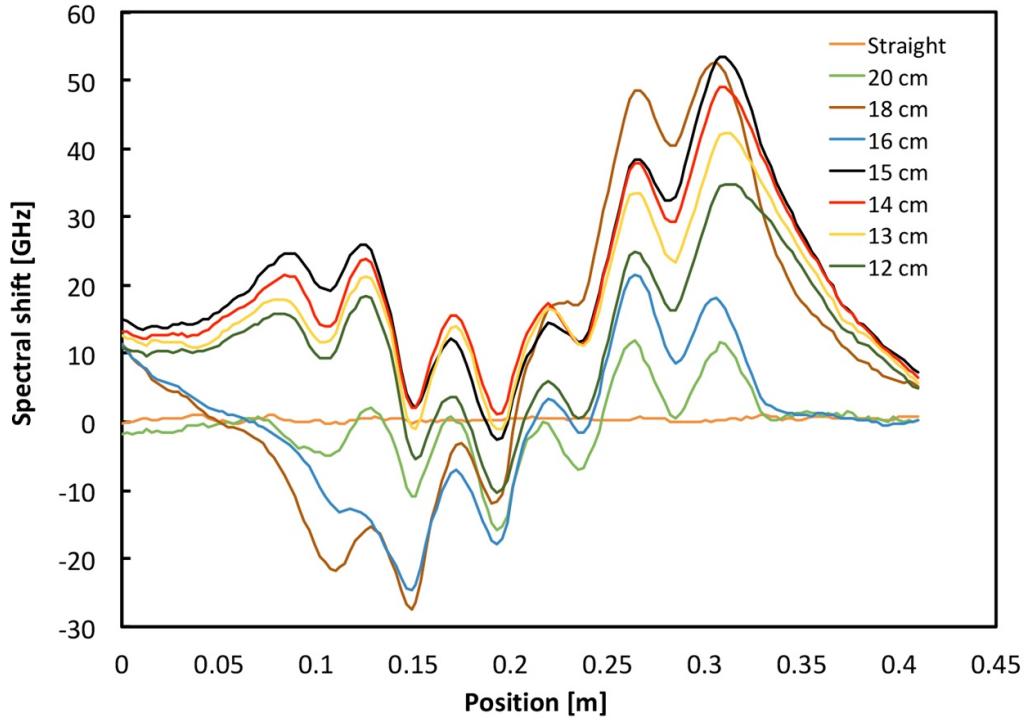

Figure 10. Spectral shift in optical fiber #1 measured at room temperature along the length of the fiber at different bending diameters of sample CORC®-O.

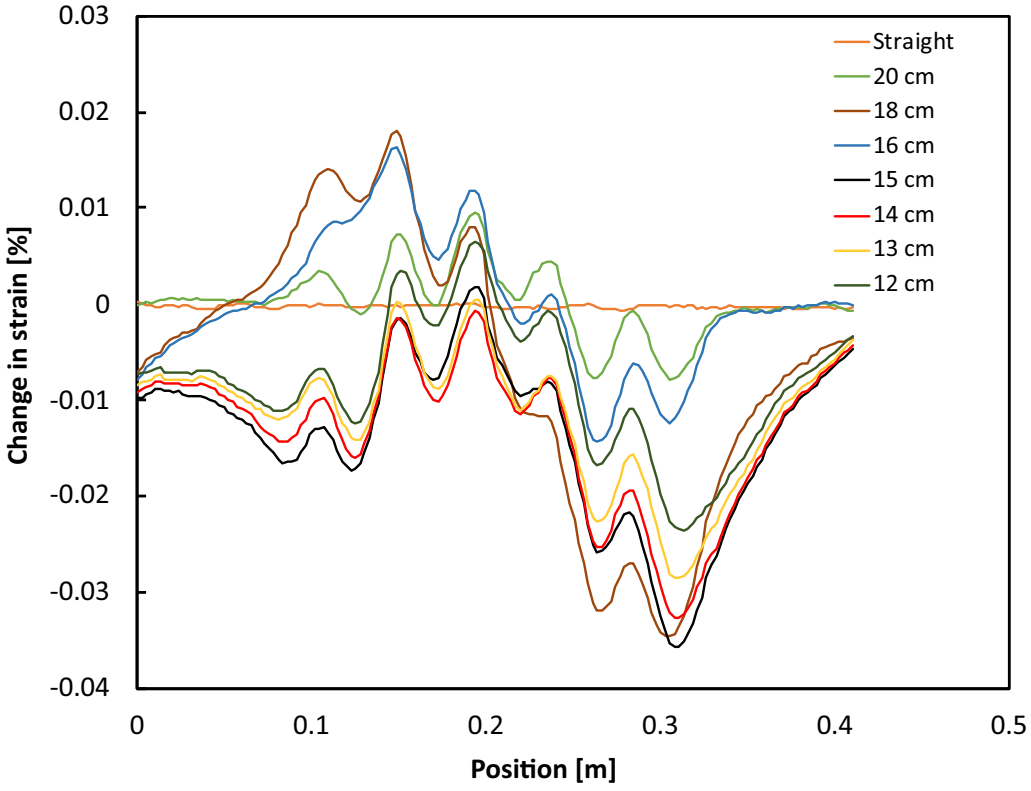

Figure 11. Change in local strain state along the length of the fiber determined from the spectral shift at different CORC® wire bending diameters of sample CORC®-O.

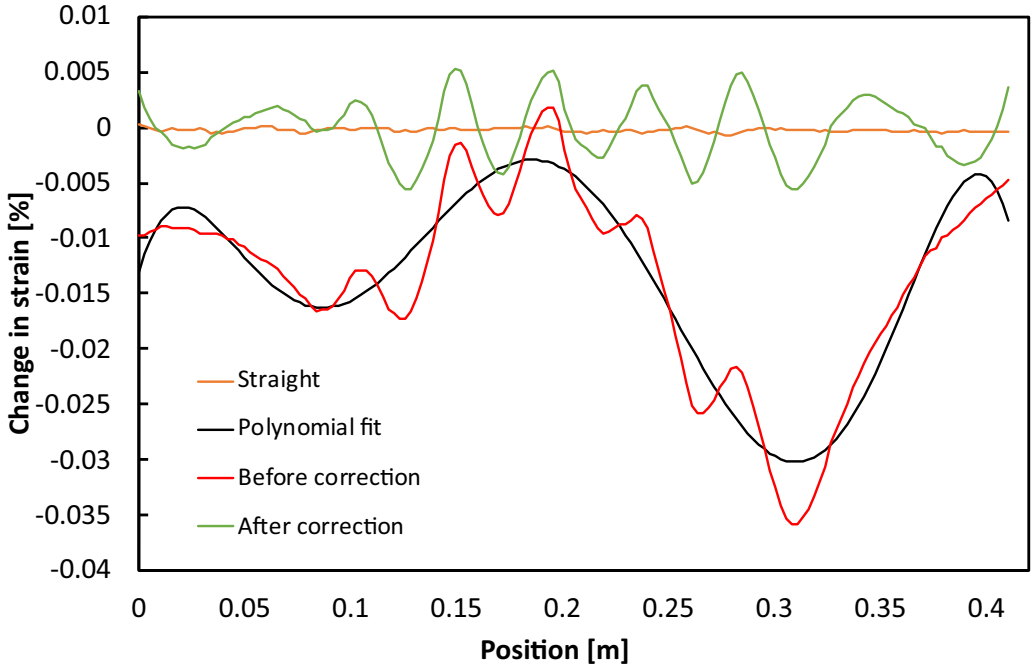

Figure 12. Change in local strain state within the fiber at room temperature at a bending diameter of 15 cm before and after correcting for the baseline. The baseline is corrected by subtracting the polynomial fit from the original spectral shift.

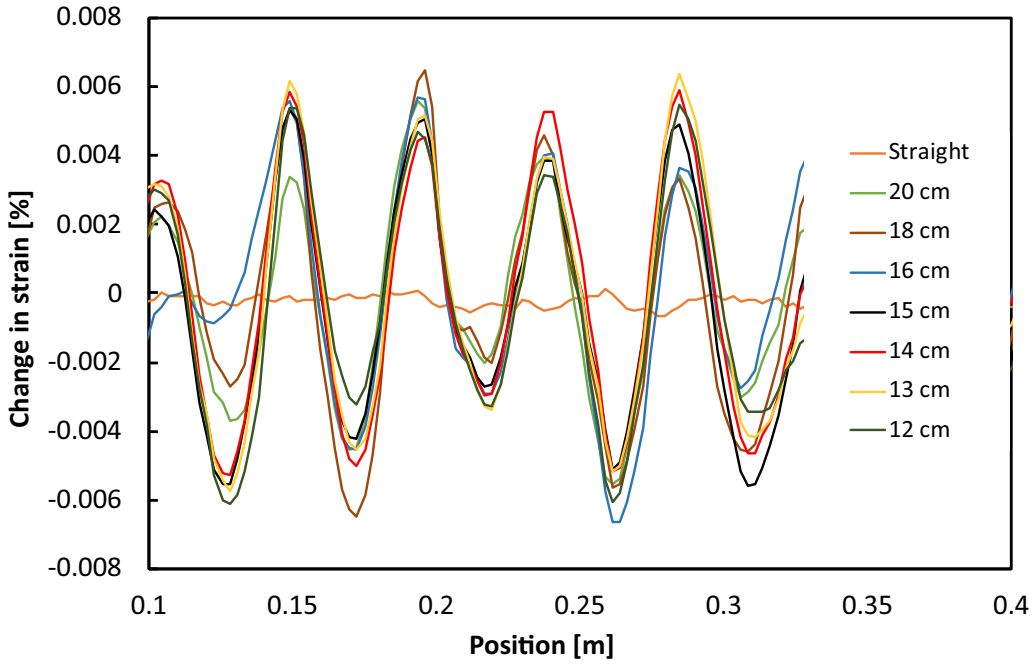

Figure 13. Change in local strain state within the fiber between the CORC® wire terminations after the data was corrected for the change in baseline.

in liquid nitrogen before the CORC® wire was bent. The first experiment used the two smaller aluminum current adapters (see figure 5(a)). Current in the CORC® wire was ramped at a constant rate of 10 A s^{-1} to 430 A, which is about 127% of I_c at 77 K. The current was kept constant at 430 A for 10 s, after which it was ramped down to 0 A. The spectral shift along the length of fiber #1 was measured while the current was ramping; the resulting spatial spectral shift map as a function of time is shown in figure 14(a). A clear increase in temperature was measured at the location of the current adapters ($x = 0.025$–0.075 and $x = 0.35$–0.4 m). The actual change in temperature was not calculated because a temperature calibration of the fiber within the CORC® wire was not performed. The experiment was repeated after one of the small current adapters was replaced by a larger copper adapter (figure 5(b)). The spectral shift as a function of time at which

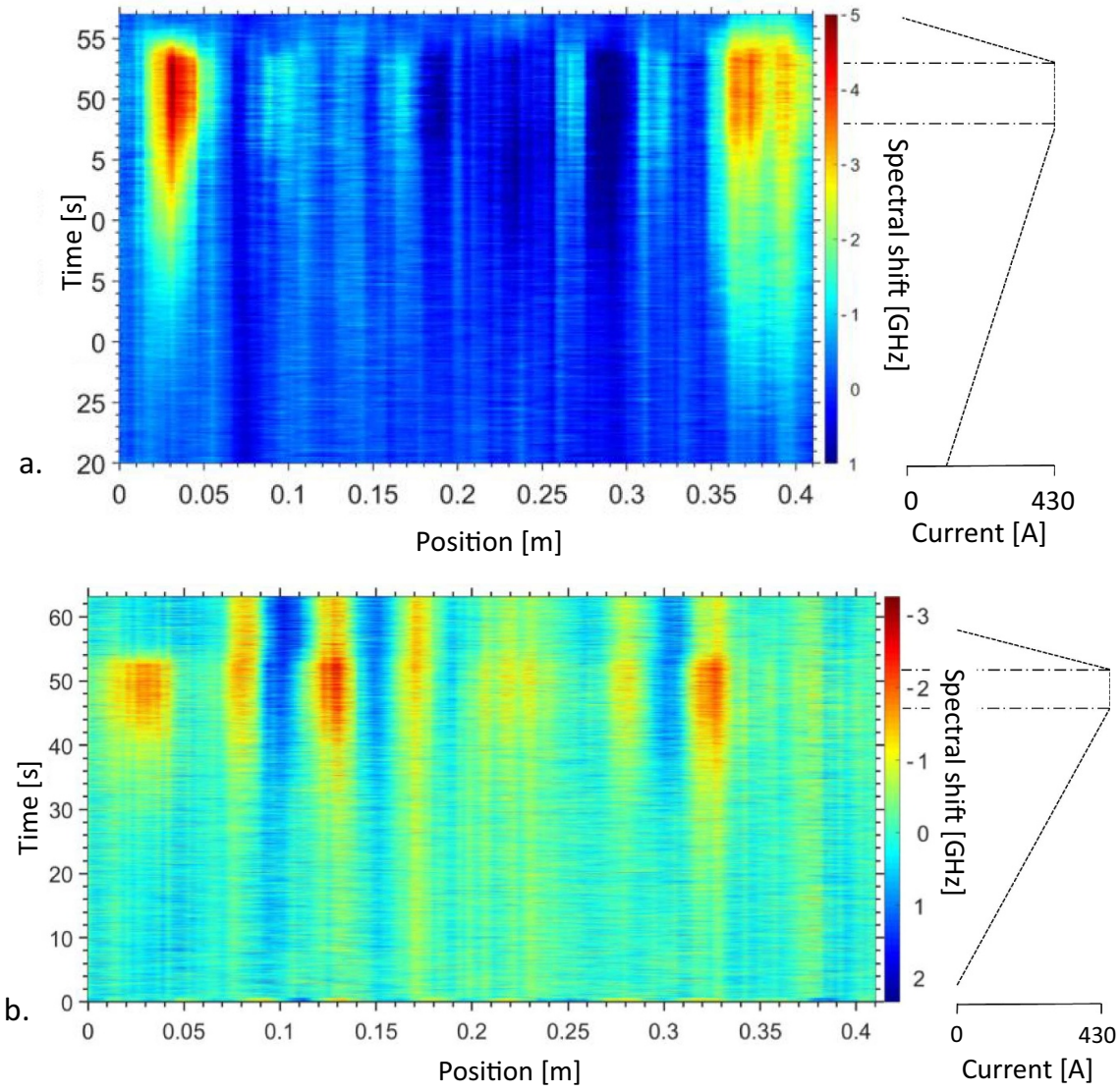

Figure 14. Spectral shift in optical fiber #1 as a function of time and position along the fiber during the time the CORC® wire carried a transport current in liquid nitrogen. (a) Small aluminum current adapters were used, and (b) a small aluminum adapter and a large copper adapter were used. The current profile as a function of time is also shown. The peak current was 430 A, which is about 127% of I_c.

current was injected into the CORC® wire is shown in figure 14(b). Heating in the termination attached to the larger copper adapter was reduced significantly while heating at the location of the smaller adapter, although reduced slightly, remained.

Figure 15 shows the spectral shift along the fiber at three different time intervals corresponding to transport currents of 10, 150, and 430 A, when the two smaller aluminum current adapters were used (figure 5(a)). Some regions between the terminations show a positive spectral shift, while other locations experience a negative shift of similar magnitude, with a periodicity of about 40 mm. Such opposite shifts are most likely caused by a change in local strain state of the fiber. A small change in local strain state of 0.0007% is enough to cause a spectral shift of 1 GHz. The change in spectral shifts of between −1.5 and 1.5 GHz between the terminations are thus likely caused by a combination of changes in local strain state induced by the Lorenz force on the CORC® wire during energization and local temperature increases. A more detailed study of the origin of spectral shift signal in CORC® cables at different conditions can be found in [34]. The much larger spectral shift at the locations of the current adapters is clearly caused by local Joule heating.

3.4. Detection of hot spots in CORC® wires with optical fibers

One of the optical fibers (fiber #2) in sample CORC®-O was used to monitor the change in temperature along the CORC® wire when overcurrent operation induced a local hot spot. The CORC® wire was bent to 11 cm diameter and contained two large copper current adapters. Current in the CORC® wire was increased at a rate of 10 A s^{-1} and held constant at 470 A (140% of I_c) for 3 s. The spectral shift as a function of time and location is shown in figure 16, where it can be seen that

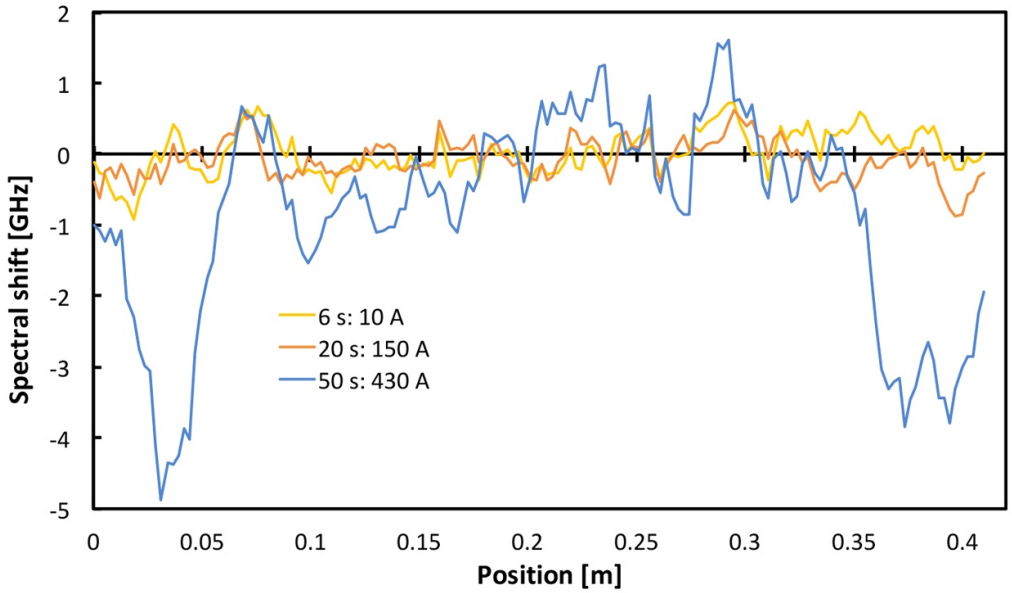

Figure 15. Spectral shift along fiber #1 at 77 K for three different times and sample currents. Two small aluminum current adapters were used during the measurement.

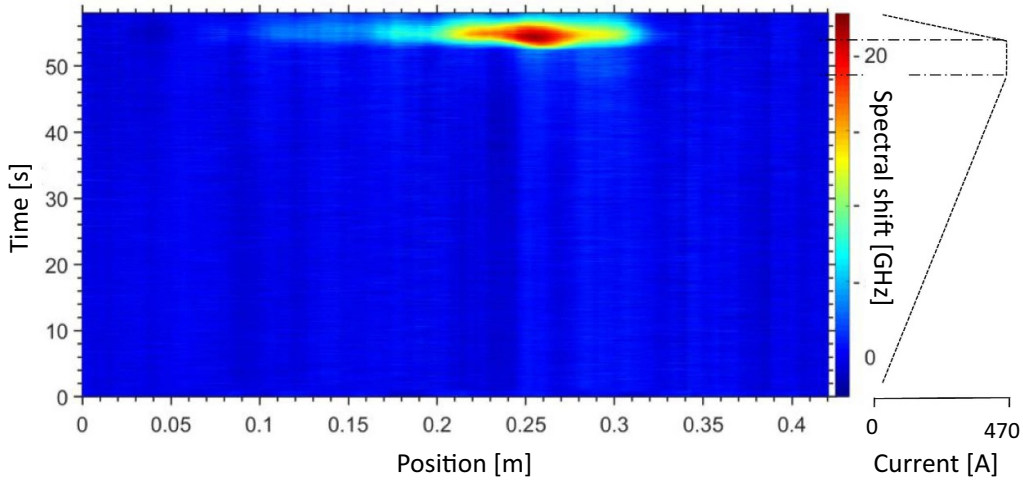

Figure 16. Spectral shift in fiber #2 in sample CORC®-O as a function of time and position along the fiber while current is ramped to 470 A (140% of I_c) in liquid nitrogen. The current profile as a function of time is also shown.

the CORC® wire developed a hot spot around $x = 0.26$ m after about 1–2 s at a current of 470 A. The current was quickly ramped down to prevent sample burn-out.

The spectral shift at location $x = 0.26$ m is plotted as a function of time in figure 17 together with the voltage measured over the CORC® wire using external voltage contact V1. The dashed lines in the figure indicate the time at which I_c of the CORC® wire was reached ($t = 38$ s). The optical fiber detected an increase in temperature after I_c had been exceeded, at which time the voltage over the sample approached 2 mV (figure 17(b)). The kink in the voltage at about 2 mV is caused by the current no longer increasing after reaching its plateau at 470 A ($t = 47$ s).

Optical fibers were also used to detect the development of a hot spot in the CORC® wire when induced by a local heater in liquid nitrogen. Current in the CORC® wire was ramped at a constant rate of 10 A s^{-1} to 430 A (127% of I_c), after which the heater was powered at 16 W for 2 s. Figure 18 shows the spectral shift as a function of time and position. No significant heating was detected until the heater was fired at $t = 46.9$ s. The hot spot propagated from the location of the heater ($x = 0.2$ m) and covered the entire CORC® wire length before the heater was switched off (t = 49 s) and the current was ramped down ($t = 56$ s).

Figure 19 shows the voltage measured over the CORC® wire with external contacts V1 and V2 as a function of time. The sample voltage reached about 0.8 mV at the time the current plateau was reached. The voltage increased slowly during the time the current was kept constant at 430 A, and increased sharply within 0.1 s after the heater was powered. The sample voltage reached 70 mV by the time the current was switched off. The ability to operate the CORC® wire at such high voltage without causing any damage or burnout is in part due to the ability of the tapes in the CORC® wire to share

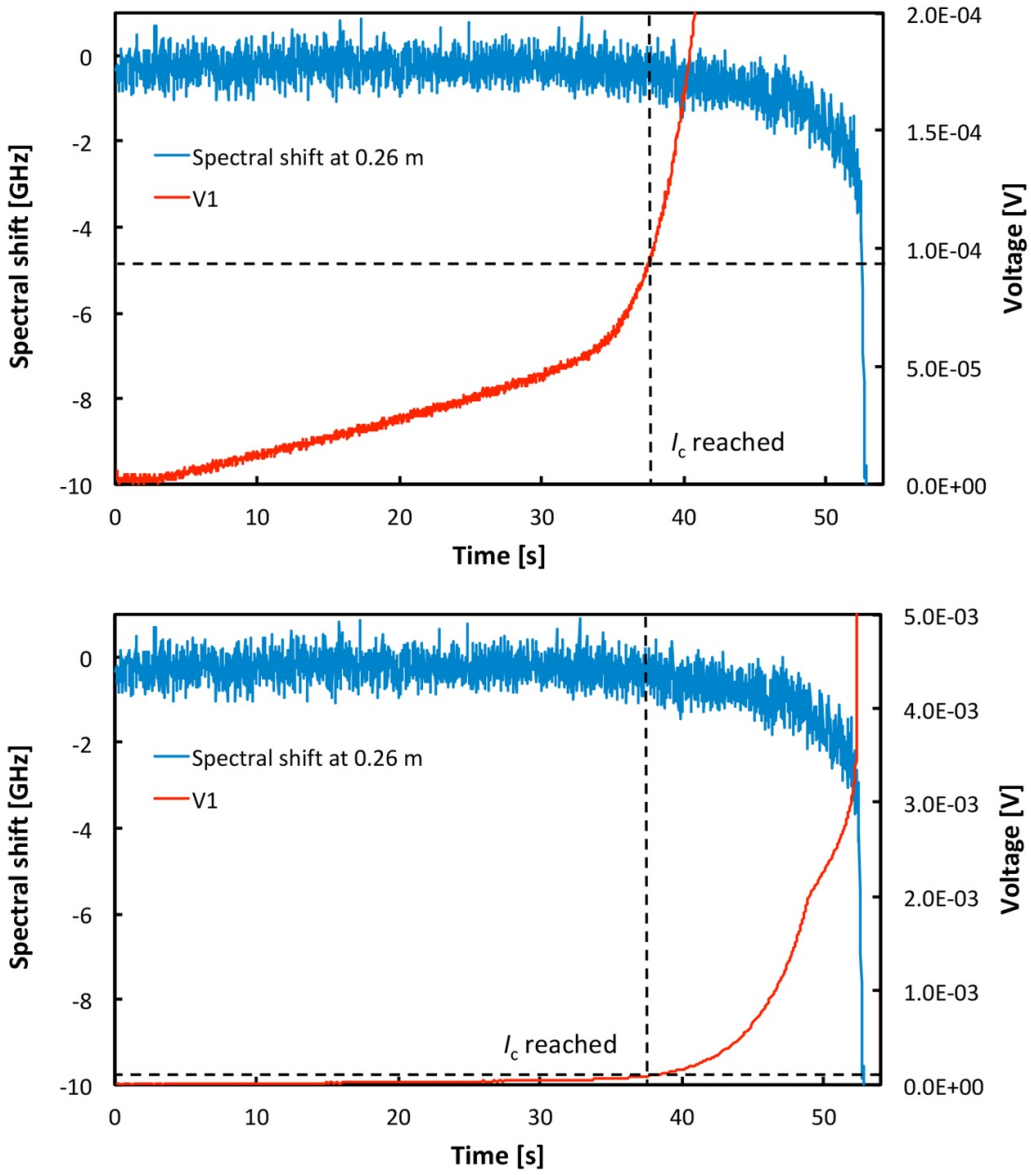

Figure 17. (a) Spectral shift as a function of time in fiber #2 at location $x = 0.26$ m in sample CORC®-O in liquid nitrogen. The voltage over the CORC® wire measured as a function of time using contact V1 is also included. Current is increased to 470 A, or 140% of I_c, and held constant at 470 A for 3 s. The dotted lines indicate the time at which the critical current of the CORC® wire is reached. (b) Voltage shown on larger voltage scale.

current with the copper core, and in part because the liquid nitrogen provided sufficient cooling. The high level of cooling also likely caused the delay between the CORC® wire exceeding I_c and the optical fiber detecting a significant change in local temperature.

3.5. Quench detection in long CORC® wires with integrated voltage contacts

The ability to detect quenches in CORC® wires with voltage contacts was investigated using CORC® wires with lengths of 0.47 m (CORC®-VS) and 5.1 m (CORC®-VL) that each contained external voltage contacts (V1 and V2) and integrated contacts (V3 and V4). Heaters covering different lengths of the sample (5 mm and 50 mm) were used to create hot spots of different sizes with respect to the CORC® wire length. The voltage wires were then used to detect the heater-induced hot spots and the quality of the voltage signal was analyzed. The short CORC® wire contained a longer heater, resulting in a hot spot size of about 11% of the sample length, while the long CORC® wire contained both a short heater (0.1% of the sample length) and long heater (1% of sample length). All measurements were performed in liquid nitrogen. An external quench detector was used to switch off the current as soon as the sample voltage, measured with the integrated voltage contacts V3, exceeded a threshold ranging 2–5 mV.

A comparison between the voltages measured by the external voltage contacts (V2) and internal voltage contacts (V3) was made with the straight, short sample CORC®-VS. A constant current of 345 A (85% of I_c at 76 K) was applied

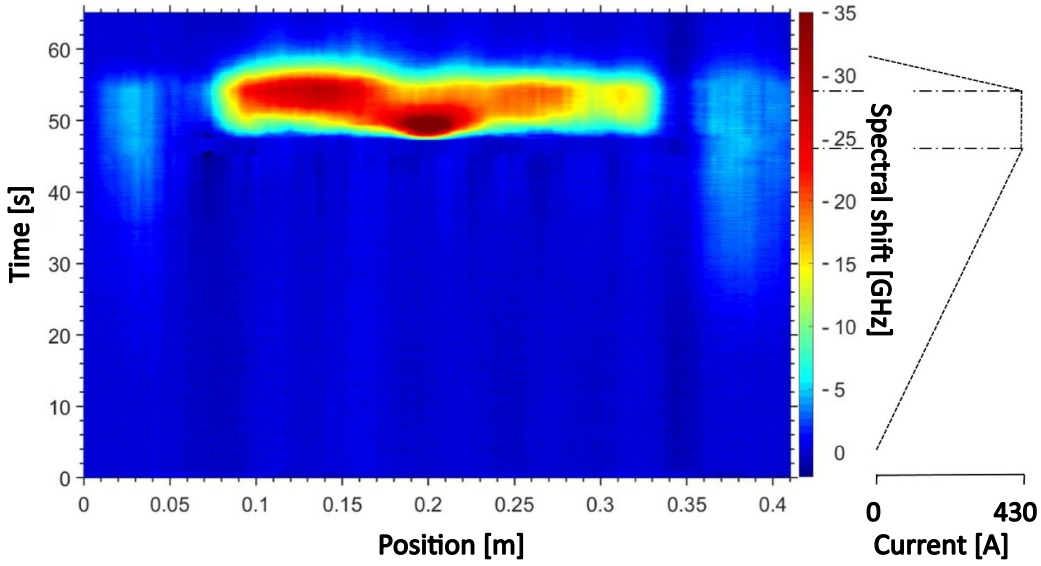

Figure 18. Spectral shift in fiber #1 as a function of time and position along the fiber during the time the CORC® wire carried a transport current and when the heater was fired in liquid nitrogen. The current profile as a function of time is also shown. The peak current was 430 A (127% of I_c).

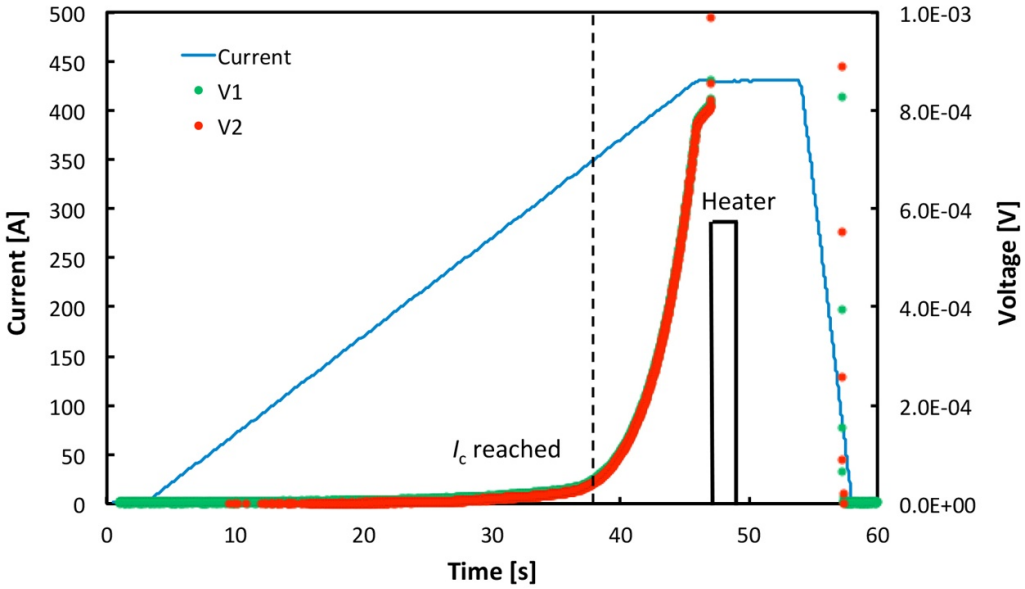

Figure 19. Current and voltage of sample CORC®-O as a function of time, measured in liquid nitrogen. The dashed line on the left indicate the time at which the CORC® wire reached I_c.

to the CORC® wire, while the heater was powered at 5.5 W. Figure 20 shows the voltage as a function of time for both voltage contacts V2 and V3 after the resistive voltages associated with the terminations ($V2_{term}$ and $V3_{term}$), which is the voltage just before the heat pulse, were subtracted from the data. The external voltage contacts contained some EMI as soon as the heater was switched on. Both voltage contacts had sufficient resolution to detect the local hotspot of 50 mm in length, corresponding to a critical voltage of 0.005 mV.

The same experiment where the 50 mm long heater provided a heating power of 5.5 W was performed on the 5.1 m long coiled CORC® wire, while it carried a current of 345 A. The voltage measured with the external contacts (V2) contained much more noise than that measured with the internal voltage contacts V3 (figure 21), because the coiled sample formed a large pickup loop. The external voltage contacts were not sensitive enough to detect the initial superconducting transition at the critical voltage of 0.005 mV over the 50 mm long hotspot, while the critical voltage was about 5 times the noise floor measured with the integrated voltage contacts (figure 21(b)).

A heater pulse of 6 W was also applied to the 5.1 m long CORC® wire using the 5 mm long heater. Figures 21(c) and (d) show the voltages measured with the external (V2) and internal

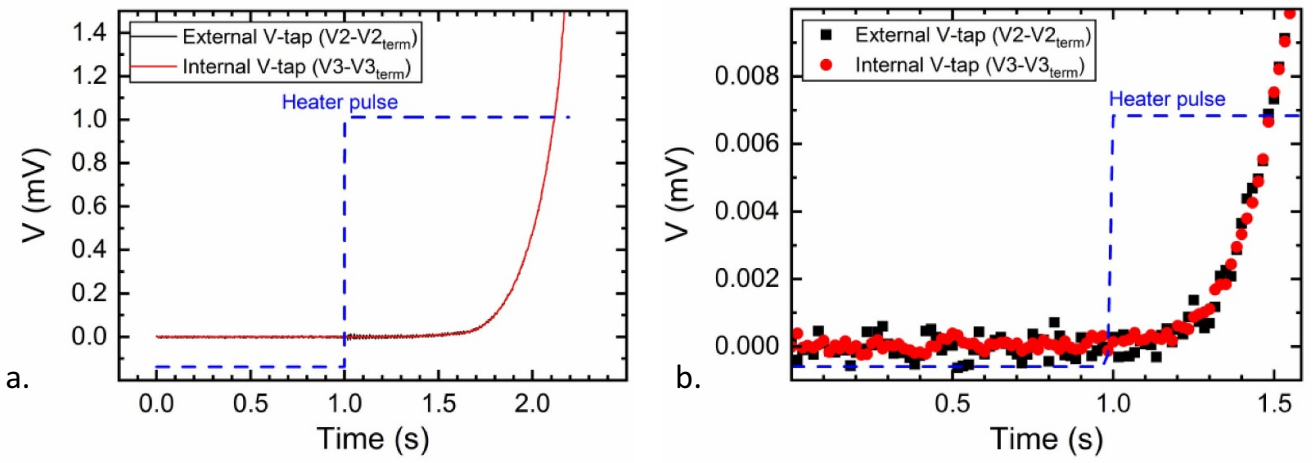

Figure 20. (a) Voltage as a function of time measured at 76 K over the 0.47 m long CORC® wire carrying a constant current of 345 A while a heat pulse of 5.5 W is applied using the 50 mm long heater. (b) The same data plotted at a different voltage scale.

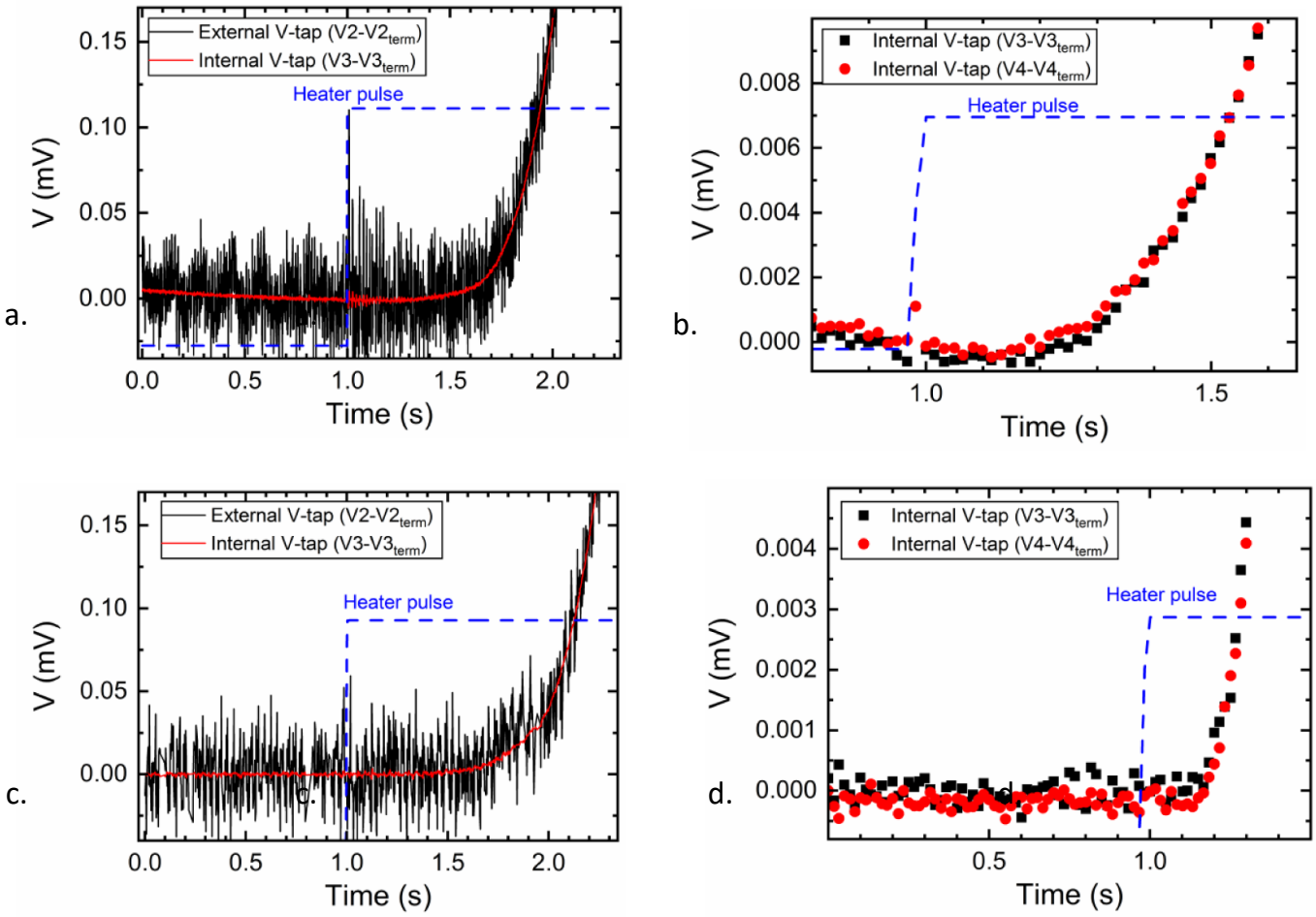

Figure 21. (a) Voltage as a function of time measured at 76 K over the 5.1 m long CORC® wire carrying a constant current of 345 A while a heat pulse of 5.5 W is applied using the 50 mm long heater. (b) Voltages measured with two pairs of integrated voltage contacts when powering the 50 mm long heater. (c) Voltage as a function of time measured at 76 K over the 5.1 m long CORC® wire carrying a constant current of 355 A while a heat pulse of 6 W is applied using the 5 mm long heater. (d) Voltage measured with two pairs of integrated voltage contacts when powering the 5 mm long heater.

(V3) voltage contacts as a function of time around when the 5 mm long heater was powered, while the CORC® wire carried a current of 355 A. The critical voltage of 0.0005 mV, that reflects the hot spot length, was just above the noise floor of the measurement taken with the integrated voltage contacts. The voltage rise occurred within about 0.25 s after the short heater

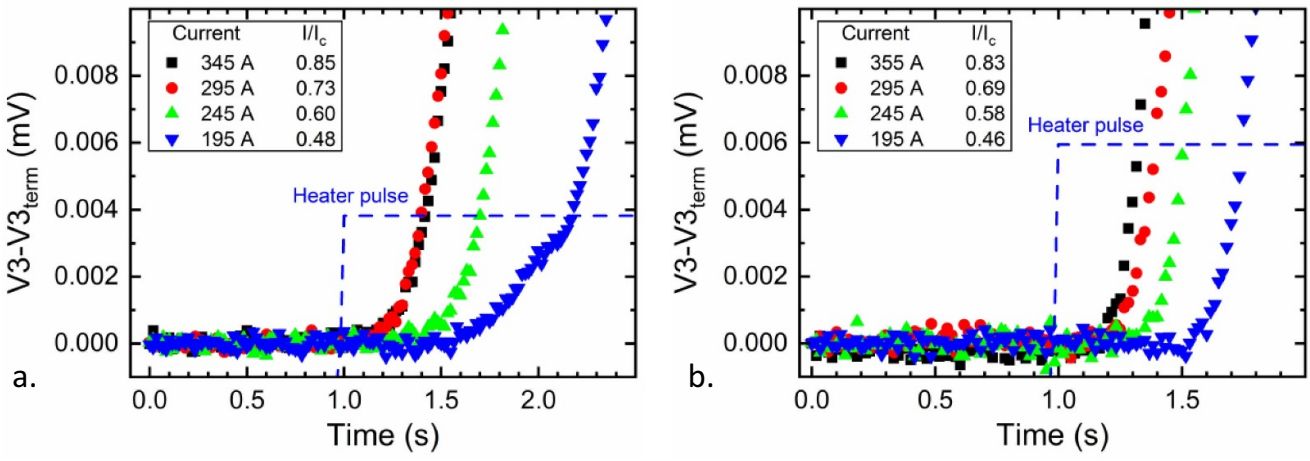

Figure 22. (a) Voltage measured with internal voltage wires as a function of time at 76 K over the 5.1 m long CORC® wire for different currents while a heat pulse of 5.5 W is applied using the 50 mm long heater, and (b) when the 5 mm long heater was powered at 6 W.

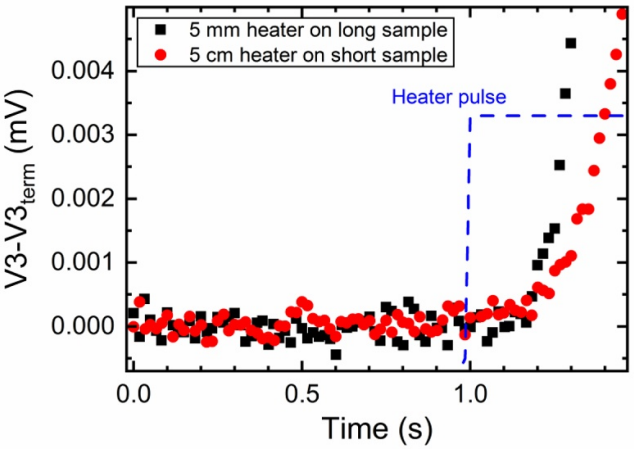

Figure 23. Voltages measured at 76 K with integrated contact V3 as a function of time measured over the 0.47 m long and 5.1 m long CORC® wires carrying a constant current of 340 A. A heat pulse of 5.5 W is applied to the short CORC® wire using the 50 mm long heater and 6 W using the 5 mm long heater on the long CORC® wire.

was power, compared to about 0.5 s for the longer 50 mm heater. The power of the short heater was concentrated in a shorter section of the CORC® wire, resulting in a more rapid increase in local temperature.

Figure 22(a) shows the results of the quench experiments performed on the 5.1 m long coiled CORC® wire using the 50 mm long heater at 5.5 W of power at different transport current levels. The time it takes for the hot spot to develop depends on the transport current. At the lowest current of 195 A, a kink in the superconducting transition can be seen after the heater was fired. This was likely caused by the hot spot first developing within the outer tape layers of the CORC® wire, and only reaching the inner layers after another 0.6 s. Figure 22(b) shows the result when the 5 mm long heater was powered at 6 W. Contrary to what was observed using the longer heater, there's no kink visible within the superconducting transition at a transport current of 195 A because the heating power is now concentrated in a much smaller CORC® wire section and all layers in the CORC® wire experience a temperature rise at roughly the same time.

Figure 23 compares the voltages measured with the internal voltage contacts (V3) of the short, straight CORC® wire (sample CORC®-VS) and the long, coiled CORC® wire (sample CORC®-VL). Both samples carried about 340 A of current when the heater pulse was applied. The data is shown using the 50 mm long heater inducing the hot spot in the short sample and the 5 mm long heater for the long sample. This provides a direct comparison between the cases in which the hot spot covers 11% and only 0.1% of the sample length. By integrating the voltage wires within the CORC® wire, sources of EMI are not attenuated with sample length allowing the noise floor to remain at the same level. This clearly demonstrates that the use of internal voltage contacts for detecting quenches due to small hotspots in long multi-tape HTS carrying a constant current allows for accurate quench detection.

3.6. Quench detection in CORC® wires at high current ramp rates

The relatively large inductive voltages that may develop over the magnet winding during energization poses a potential challenge for quench detection using voltage measurements. Integrated voltage wires have the advantage of minimizing inductive offset voltages, making them likely suitable for quench detection even at high current ramp rates. Figures 24(a) and (b) compare the voltages measured with the external (V2) and integrated voltage wires (V3) of the 0.47 m long (CORC®-VS) and 5.1 m long (CORC®-VL) CORC® wires during current ramp rates ranging from 5 A s^{-1} to 2000 A s^{-1}. The inductive voltage measured with external contacts on the long, coiled sample was about 20–30 times higher than that of the shorter, straight CORC® wire. The voltage over both samples also showed large oscillations at high current ramp rates at the initial stage of the current ramp.

The integrated voltage wires (V3) did not show a significant inductive voltage in either sample (figures 24(c) and (d)),

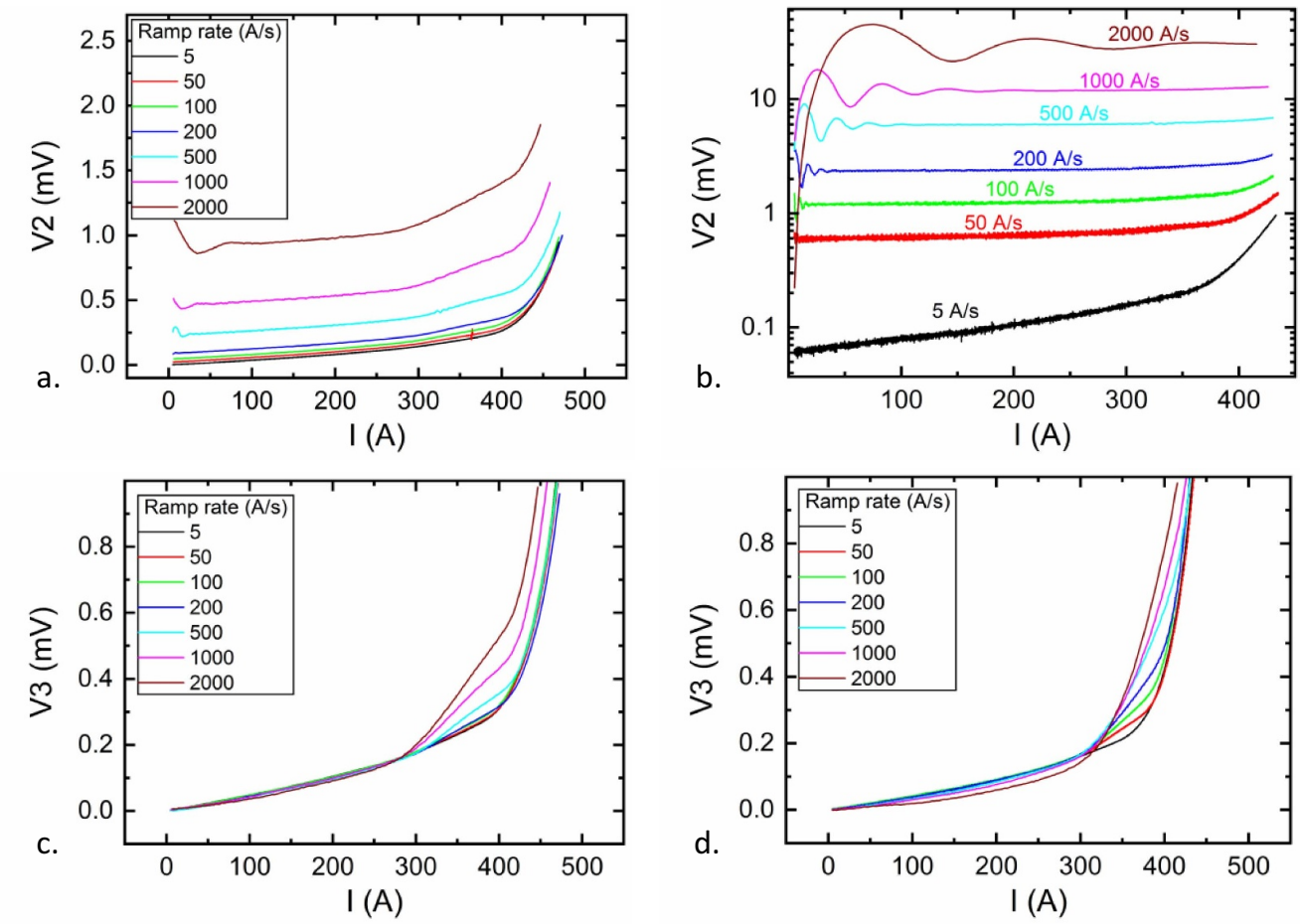

Figure 24. Voltage as a function of current measured at different current ramp rates in liquid nitrogen. (a) External voltage contacts V2 of the 0.47 m long sample CORC®-VS, (b) external voltage contacts V2 of the 5.1 m long sample CORC®-VL, (c) integrated voltage contacts V3 of the 0.47 m long sample CORC®-VS, and (d) integrated voltage contacts V3 of the 5.1 m long sample CORC®-VL.

because the inductive pickup loop was minimized. Voltage oscillations were also not observed, even at the highest current ramp rate of 2000 A s^{-1}. The voltage measured over the short sample (CORC®-VS) showed a distinct kink at a current of around 300 A, which became more pronounced at current ramp rates exceeding 200 A s^{-1}. Such a kink was also observed in the voltage measurement of the longer sample (CORC®-VL), where it appeared at a current ramp rate as low as 50 A s^{-1}. The superconducting transition would start at 300 A at high current ramp rates exceeding 500 A s^{-1}, instead of about 380–400 A.

A quench was induced during subsequent tests using a heater at the same time the sample current was ramped at a constant rate. This experiment resembles the case where a magnet is being ramped to field while a local hot spot develops in the cable. Figure 25 shows the voltage measured over the 5.1 m long CORC® wire (CORC®-VL) using the external (V2) and integrated (V3) voltage contacts at the time the current was increased at rates of 50 A s^{-1} and 200 A s^{-1}. As expected, the external voltage contacts included more noise and a significant inductive voltage that exceeded 2 mV at a ramp rate of 200 A s^{-1}. The 5 mm long heater was powered at 6 W as soon as the current exceeded about 250 A. Both the external and internal voltage contacts measured the superconducting transition at about 330 A caused by the local hot spot. The experiment clearly shows that the heater-induced quench can be detected in time using integrated voltage contacts, even when the sample current is changing at relatively high rate.

4. Discussion

4.1. Quench detection in CORC® wires using Rayleigh scattering in optical fibers

Rayleigh scattering in optical fibers is often described as a potential quench detection method in HTS conductors. The method is able to detect a hot spot without experiencing many of the external factors that may interfere with quench detection using voltage contacts, such as inductive voltages and EMI. The experiments performed in liquid nitrogen with the CORC® wire containing both optical fibers and voltage contacts allowed for an initial comparison of both methods regarding sensitivity and speed to detect the formation of a hot spot, although a single conductor in a liquid nitrogen bath tends to be cryo-stabilized, and therefore does not fully represent the stability behavior of a actual HTS magnet.

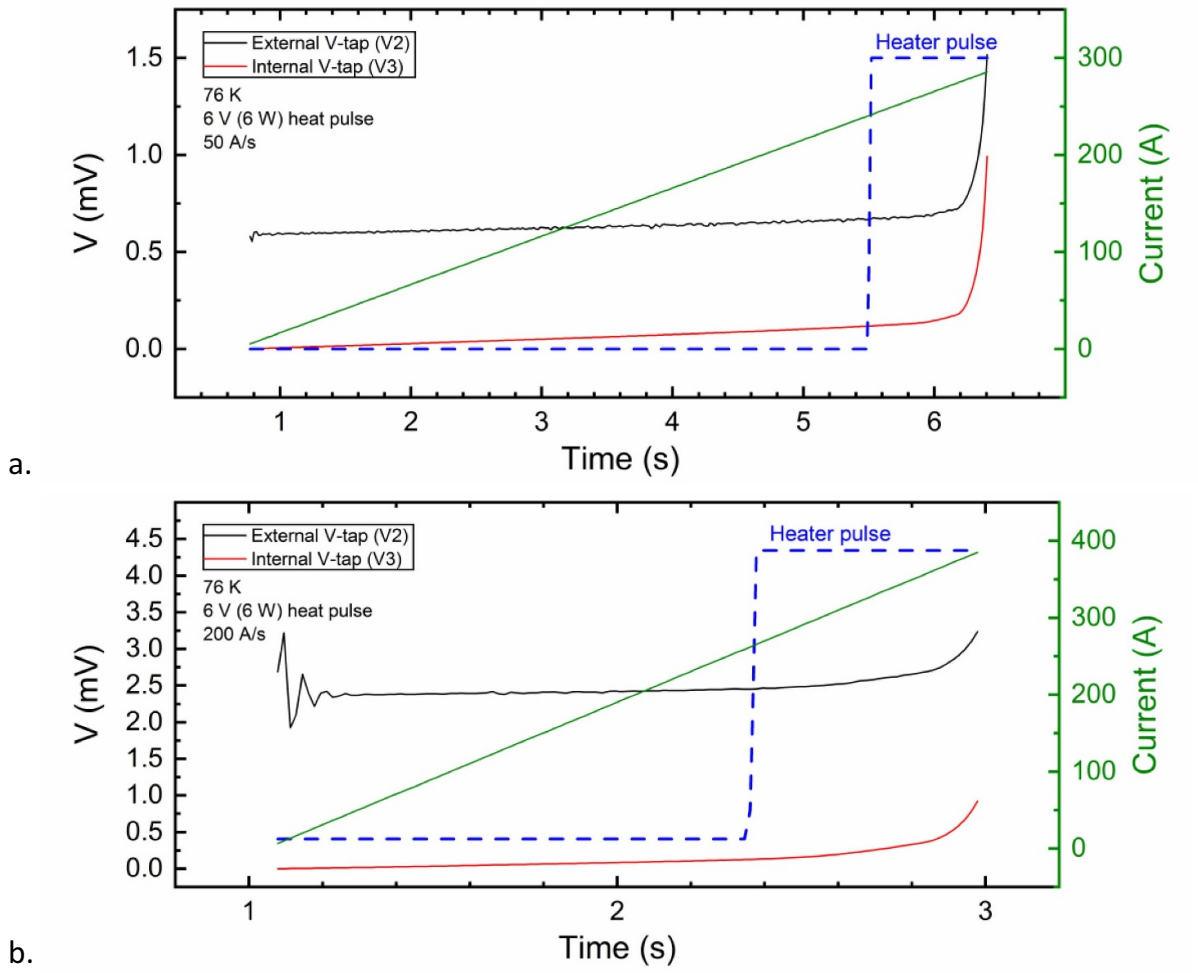

Figure 25. Voltages measured using the external (V2) and integrated (V3) voltage contacts at 76 K of the 5.1 m long CORC® wire (CORC®-VL) at (a) at a current ramp rate of 50 A s^{-1} and (b) at a current ramp rate of 200 A s^{-1}. The 5 mm long heater is powered at 6 W once the current has reached about 250 A.

The first comparison is made for the case in which current in the CORC® wire was ramped at a constant rate to exceed I_c, and then held constant. Figure 17 shows that the spectral shift at the location where the hot spot developed ($x = 0.26$ m) only changes significantly above the noise floor about 8–10 s after the critical current had been exceeded. A significant temperature increase associated with the hot spot was only detected once the current reached 140% of I_c, at which time the sample voltage had reached about 2 mV. Dissipation due to the transport current in the CORC® wire was about 0.68 W, which was not sufficient to cause a significant increase in hot spot temperature when the sample experienced ample cooling from the liquid nitrogen. These results are in contrast to prior results using optical fibers for which the optical fiber was in more intimate contact with the conductor [12, 14].

The response of the optical fibers to the development of a hot spot was much faster when the hot spot was initiated by a high-power heater while the current in the CORC® wire exceeded I_c. Figure 26 compares the spectral shift in optical fiber #1 at the location of the hot spot with the voltage measured over the CORC® wire terminations while the sample current was increased and the heater was powered. Figure 26(a) shows the superconducting-to-normal transition of the CORC® wire at $t = 37$ s, as measured with the voltage contacts. The sample voltage increased from about 0.7 mV to 1 mV (left arrow in figure 26(b)) within 0.15 s after the heater was switched on at $t = 46.9$ s, which is the typical voltage level at which the quench protection circuit would be activated when operating CORC® cables. The spectral shift at the location of the hot spot increased from 0 ± 0.5 GHz to -2.5 GHz after an additional 0.25 s after the voltage reached 1 mV (right arrow). Such change in spectral shift was large enough that it could be used to trigger the quench protection circuit. At that time, again indicated by the right arrow, the voltage over the CORC® wire had reached 23 mV.

The difference in response time between voltage measurements and the change in spectral shift in embedded optical fibers to the development of a heater-induced hot spot could have several origins. The effective cooling of the liquid nitrogen and the relatively low current density in the copper cross-section in the CORC® wire of 80 A mm^{-2} slows the increase in temperature at the hot spot. Also, the separation of the fibers from the tapes in the outer layers, which will transition

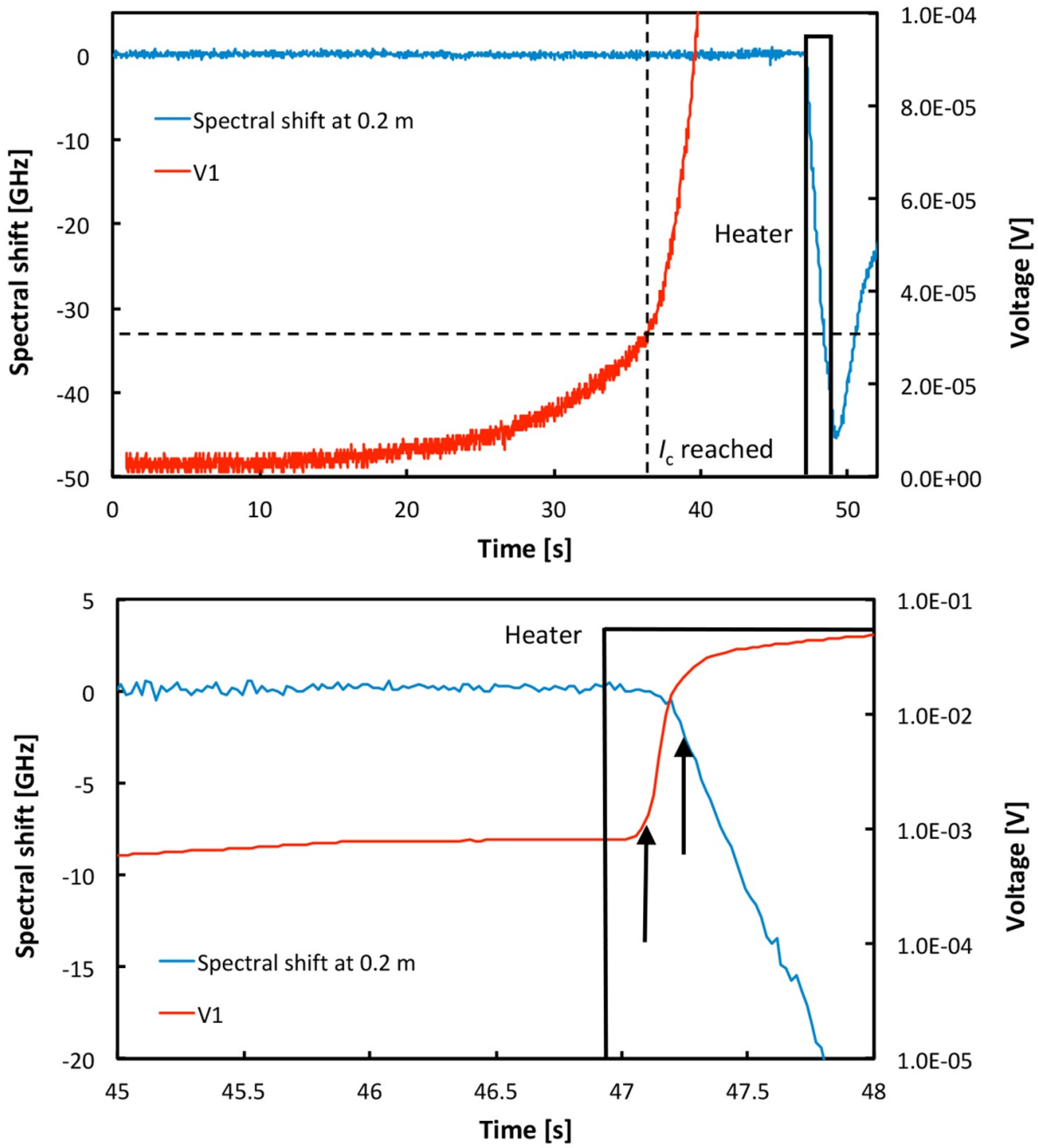

Figure 26. (a) Spectral shift of fiber #1 in the straight CORC® wire (CORC®-O) at the location of the heater ($x = 0.2$ m) and voltage measured with contact V1 as a function of time in liquid nitrogen. The current was increased to 430 A and a spot heater was powered at 16 W for 2 s. The dotted lines indicate the time at which the critical current of the CORC® wire was reached and when the spot heater was engaged. (b) Spectral shift and voltage shown on different scales. Arrows indicate the voltage and spectral shift at which the quench protection circuit could be triggered for each technique.

first when the heater is fired, will cause a time delay. The response time of the optical fiber to a quench could thus likely be reduced when the fiber is located closer to the outer tapes, when the CORC® wire is operated at higher current densities, or when the cooling is less efficient. Additional tests at current densities relevant for high-field magnet applications and at operating currents in the range of 50%–70% of I_c are required to determine whether quench detection using Rayleigh scattering in optical fibers is a viable method for use in superconducting magnets. Furthermore, improvements in the fiber integration within the CORC® wire are also expected to improve the optical fiber response time.

Another potential concern with using Rayleigh scattering in optical fibers to detect quenches in magnet conductors is its much higher sensitivity to change in local strain than to a change in temperature. A change in strain state of only 0.1% that's likely to occur during magnet ramping would already result in a spectral shift of 146 GHz. The response to strain of

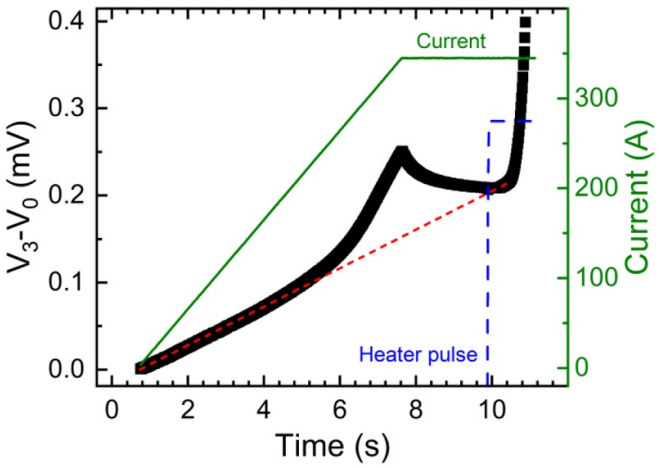

Figure 27. Voltage and current as a function of time measured using internal voltage contacts V3 over the 5.1 m CORC® wire (CORC®-VL) at 76 K during a constant current ramp rate of 50 A s^{-1}. The current was kept constant once it reached 340 A. The dashed line indicates the voltage associated with a constant contact resistance.

the optical fiber could potentially mask the development of a hot spot during ramping. Methods to distinguish between the spectral shifts associated with a change in temperature from a strain-induced change need to be developed and incorporated into the real-time quench detection logic.

4.2. Current distribution in CORC® wires at high current ramp rates

The voltage measurements performed with the integrated voltage contacts at different current ramp rates provides us with important new insight about current distribution in CORC® wires. At relatively low current ramp rates, current distribution between the tapes in CORC® wires, and other multi-tape superconducting cables, is mainly determined by the contact resistances between the tapes and the cable terminations [35]. Inhomogeneous current distribution occurs when these resistances vary and tapes with the lowest overall contact resistance carry the majority of the current. Only once current in these tapes exceed I_c, and the voltage generated over the tapes is sufficient to overcome the higher contact resistance experienced by the remaining tapes, will these remaining tapes carry their share of the overall current. Such behavior typically causes a distinct kink in the resistive part of the *V*–*I* curve before the superconducting transition of the cable starts.

Figures 24(c) and (d) compare the voltages measured with the integrated voltage wires (V3) in both the short (CORC®-VS) and long (CORC®-VL) CORC® wire at different current ramp rates. At low current ramp rate, the resistive voltage measured over both samples was almost entirely linear until the superconducting-to-normal transition started, indicating that current was distributed evenly between tapes. On the other hand, a distinct kink in the resistive transition appeared at higher current ramp rates. The current at which the kink appeared did not depend on sample length or ramp rate and always occurred around 300 A, but the kink became more pronounced when the current ramp rate or sample length increased. The measurements indicate that the current distribution between tapes in the CORC® wire may change at high current ramp rates.

Besides being affected by the contact resistance between tapes and cable terminations, current distribution between tapes in HTS cables is also determined by the difference between tape inductances when current is ramped at high rates [36]. The inductive voltage that develops over each tape may result in a higher fraction of the current to be injected into the tapes with the lowest inductance and thus lowest inductive voltage. Because the tapes in CORC® wires are wound at different diameters and at different winding angles, the tape inductance will differ between layers in which they are wound. The current distribution in CORC® wires ramped at high current rates is thus determined by both the homogeneity of the contact resistance at the terminations, and the variation in inductance between tapes.

The inductively-driven current distribution in CORC® wires can be studied more closely when considering the voltage measured as a function of time during the current ramp and after the current was kept constant. Figure 27 shows the voltage measured as a function of time over the 5.1 m long CORC® wire after current was increased at 50 A s^{-1} and kept constant once it reached 340 A. The voltage increased linearly with time (and thus current), until it increased at a higher rate after 5 s. The increase in voltage indicates that a change in current distribution between the tapes is occurring. The difference between inductive voltages over each tape, which is constant at a constant ramp rate, now becomes the driving factor behind the current distribution. On the other hand, once the current was kept constant at 340 A ($t = 7.5$–10 s), the inductive voltages over the tapes diminished over time, and the current distribution returned to its original state. The overall sample voltage thus returned to the value corresponding to initial linear dependence on time and thus current.

Figure 28(a) shows the voltage measured over the 5.1 m long CORC® wire as a function of current for different ramp rates, where the magnitude of the sudden increase in voltage around 250–300 A clearly depends on the current ramp rate. Figure 28(b) shows the change in voltage as a function of time, where the voltage decayed to a constant value (0.2 mV) once the current was kept constant at 340 A.

The inductive voltage generated over the tapes in the CORC® wire depends on the sample length and current ramp rate. The inductance of each tape is a linear function of its length, which means that the peak voltage reached at a given current ramp rate also scales with sample length. Figure 29 shows the voltage as a function of time measured over the 5.1 m (CORC®-VL) and 0.47 m long (CORC®-VS) CORC® wires when current was ramped at 50 A s^{-1} to 340 A, after which it was kept constant. The difference between the peak voltage and the value to which it decayed after the current ramp stopped was about 0.04 mV for the 5.1 m long sample, and about 0.005 mV for the 0.47 m long sample. The difference in peak voltage scales with sample length that includes the length of the CORC® wire within the terminations.

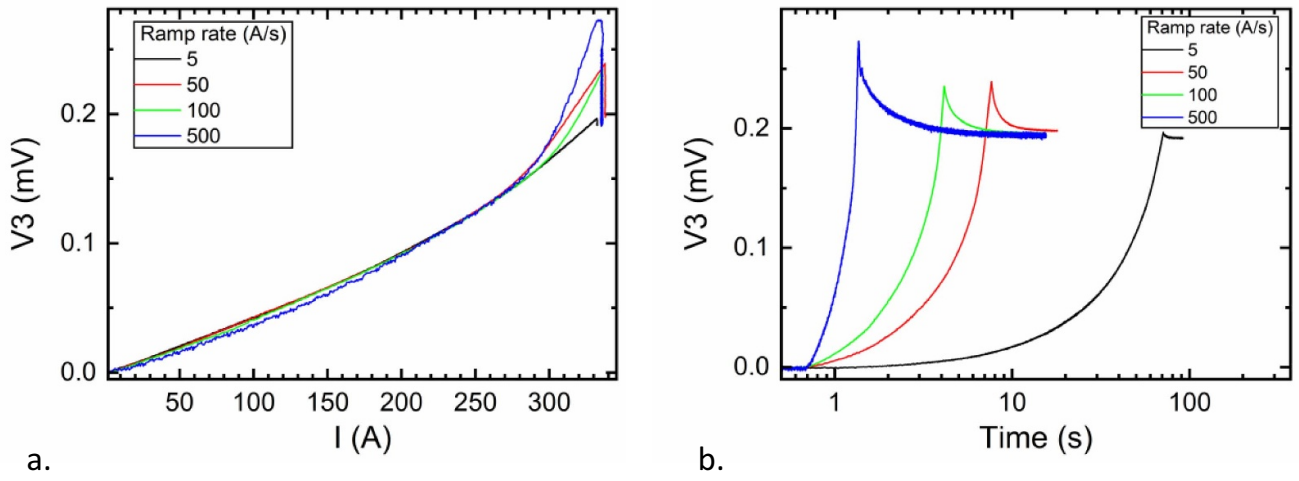

Figure 28. (a) Voltage as a function of current measured using internal voltage contacts V3 over the 5.1 m CORC® wire (CORC®-VL) at 76 K for different current ramp rates to 340 A, after which the current is kept constant. (b) The same data presented as a function of time.

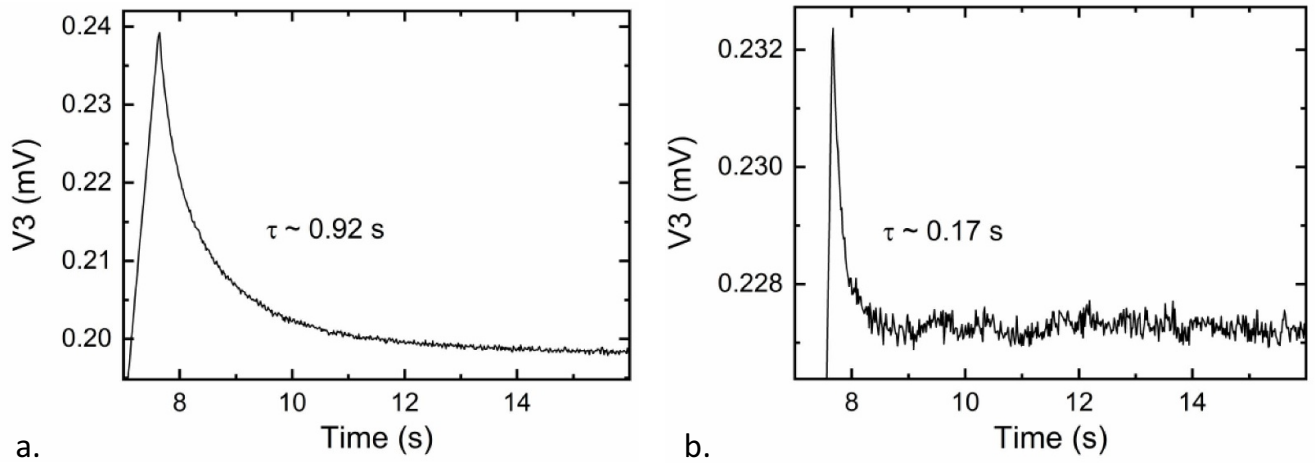

Figure 29. Voltage measured using internal voltage contacts V3 as a function of time during a constant ramp rate of 50 A s^{-1} to 340 A, after which the current is kept constant, (a) for the 5.1 m CORC® wire, and (b) the 0.47 m CORC® wire.

The time constant at which the voltage decayed after the current ramp was stopped also depends on the inductance and thus on sample length. This is confirmed in figure 29(b) where the time constant determined from the voltage decay is shown. The decay time (τ) for the long sample is about 5.4 times that of the short sample, which is again comparable to the ratio of the sample lengths when taking the CORC® wire length within the terminals into account.

The voltages measured at high current ramp rates over a relatively long CORC® wire clearly demonstrated how current distribution between tapes may be affected by the difference in tape inductance. A change in current distribution due to inductive voltages typically is not observed in shorter samples, because the overall inductive voltage remains relatively low compared to the voltages associated with the contact resistances between the tapes and the terminations. The results highlight the importance of limiting the range over which the tape inductances in CORC® wires vary when long CORC® wires are applied in applications that may operate at relatively high current ramp rates. As shown in figure 24, very high current ramp rates in exceeding 1000 A s^{-1} resulted in the CORC® wire to transition into its normal state at a slightly lower current when considering the typical voltage criterion of 1 μV cm^{-1}. Although this is an inductively driven transition and the voltages would converge at higher voltage, or decay once the current would be kept constant, this effect may become more pronounced in a CORC® conductor wound from a much higher tape count.

5. Conclusions

The results presented in this paper show the versatility of CORC® wires in which the copper core not only functions as a stabilizer but also provides the opportunity to incorporate voltage wires and optical fibers. Reliable methods were developed to embed voltage wires and optical fibers within grooves that were extruded into the former and routing them out through the solder-filled terminations, although the results indicate that further optimization of the integration of optical fibers will likely be beneficial.

The integrated instrumentation allows real-time monitoring of the conductor strain, temperature, and voltage, providing a more detailed understanding of the CORC® wire operation and enabling fast and effective quench detection. Rayleigh scattering in the embedded optical fibers allowed for determination of local strain and temperature along the length of the fiber. Heating within the terminations at the location of current injection could clearly be measured. The development of a hot spot within the CORC® wire induced by overcurrent or a spot heater was also clearly detected but lagged the speed and resolution of the voltage measurements in these experiments. Operating at higher current densities in environments that provide less efficient cooling would likely improve the response time of optical fibers, as well as better integration of the fiber into the CORC® wire to allow even closer contact between the fiber and the superconducting tapes. The much higher sensitivity of the optical fiber to strain compared to temperature, and the inability to distinguish between the two sources, could be seen as a drawback of quench detection using Rayleigh scattering in optical fibers for use in high-field magnets. A change in operating strain could mask the development of a local hot spot or cause false positives.

Integrated voltage wires in CORC® wires allowed accurate voltage measurements without the influence of outside noise or inductive voltages that may develop during high current ramp rates. The voltage measurements allowed fast and accurate detection of local hot spots in a 5.1 m long coiled CORC® wire, whether they were caused by overcurrent, or a spot heater. Integrated voltage wires were able to detect a hot spot that only covered 0.1% of the CORC® wire length, even at very high current ramp rates. Reliable quench detection based on voltage measurements is thus possible in multi-tape high-temperature superconductors in which current sharing between tapes allows them to be operated within the flux flow regime.

Accurate voltage measurements with integrated voltage wires allowed the detection of inductively driven current redistribution between the tapes in a long CORC® wire at high current ramp rates. The measurements showed that minor differences between tape inductances in the CORC® wire may results in uneven current distribution in long conductors when operated at high current ramp rates. Reducing the range over which the tape inductances vary, by optimizing the winding angle of the tapes, may be needed when long CORC® conductors are operated at high current ramp rates, such as large fusion magnets.

Acknowledgment

This work was supported by the United States Department of Energy under Grant Numbers DE-SC0014009 and DE-SC0018706.

ORCID iDs

D C van der Laan https://orcid.org/0000-0001-5889-3751
J D Weiss https://orcid.org/0000-0003-0026-3049

References

[1] Larbalestier D C Jiang J Trociewitz U P Kametani F Scheuerlein C Dalban-Canassy M, Matras M, Chen P, Craig N C Lee P J and Hellstrom E E 2014 Isotropic round-wire multifilament cuprate superconductor for generation of magnetic fields above 30 T *Nat. Mater.* **13** 375–81

[2] Fajardo L G, Brouwer L, Caspi S, Gourlay S, Prestemon S and Shen T 2018 Designs and prospects of Bi-2212 canted-cosine-theta magnets to increase the magnetic field of accelerator dipoles beyond 15 T *IEEE Trans. Appl. Supercond.* **28** 4008305

[3] Yanagisawa Y, Xu Y, Iguchi S, Hamada M, Matsumoto S, Nishijima G, Nakagome H, Takao T, Suematsu H, Oshima Y and Jin X 2015 Combination of high hoop stress tolerance and a small screening current-induced field for an advanced Bi-2223 conductor coil at 4.2K in an external field *Supercond. Sci. Technol.* **28** 125005

[4] Marshall W S, Bird M D, Godeke A, Larbalestier D C, Markiewicz W D and White J M 2017 Bi-2223 test coils for high-resolution NMR magnets *IEEE Trans. Appl. Supercond.* **27** 4300905

[5] Hazelton D W, Selvamanickam V, Duval J M, Larbalestier D C, Markiewicz W D, Weijers H W and Holtz R L 2009 Recent developments in 2G HTS coil technology *IEEE Trans. Appl. Supercond.* **19** 2218–22

[6] Yoon S, Kim J, Cheon K, Lee H, Hahn S and Moon S-H 2016 26T 35 mm all-$GdBa_2Cu_3O_{7-x}$ multi-width no-insulation superconducting magnet *Supercond. Sci. Technol.* **29** 04LT04

[7] Weijers H W 2018 A marriage of high and low temperature superconductors: the 32 T magnet *MST Seminar NHMFL*, (*Tallahassee*, January 24)

[8] Song H and Schwartz J 2009 Stability and quench behavior of $YBa_2Cu_3O_{7-x}$ coated conductor at 4.2 K, self-field *IEEE Trans. Appl. Supercond.* **19** 3735–43

[9] Wang X, Trociewitz U P and Schwartz J 2009 Self-field quench behavior of $YBa_2Cu_3O_{7-\delta}$ coated conductors with different stabilizers *Supercond. Sci. Technol.* **22** 13

[10] Senatore C, Alessandrini M, Lucarelli A, Tediosi R, Uglietti D and Iwasa Y 2014 Progresses and challenges in the development of high-field solenoidal magnets based on RE123 coated conductors *Supercond. Sci. Technol.* **27** 103001

[11] Scurti F, Ishmael S, Flanagan G and Schwartz J 2016 Quench detection for high temperature superconductor magnets: a novel technique based on Rayleigh-backscattering interrogated optical fibers *Supercond. Sci. Technol.* **29** 03LT01

[12] Scurti F, Sathyamurthy S, Rupich M and Schwartz J 2017 Self-monitoring "SMART" (RE)$Ba_2Cu_3O_{7-x}$ conductor via integrated optical fibers *Supercond. Sci. Technol.* **30** 114002

[13] Scurti F, McGarrahan J and Schwartz J 2017 Effects of metallic coatings on the thermal sensitivity of optical fiber sensors at cryogenic temperatures *Opt. Mater. Express* **7** 1754–66

[14] Scurti F and Schwartz J 2017 Optical fiber distributed sensing for high temperature superconductor magnets *25th Optical Fiber Sensors Conf. (OFS)* (IEEE) pp 1–4

[15] Marchevsky M, Xie Y-Y and Selvamanickam V 2010 Quench detection method for 2G HTS wire *Supercond. Sci. Technol.* **23** 034016

[16] Marchevsky M and Gourlay S A 2017 Acoustic thermometry for detecting quenches in superconducting coils and conductor stacks *Appl. Phys. Lett.* **110** 012406

[17] Marchevsky M, Hershkovitz E, Wang X, Gourlay S A and Prestemon S 2018 Quench detection for high-temperature

superconductor conductors using acoustic thermometry *IEEE Trans. Appl. Supercond.* **28** 4703105
[18] Godeke A, Cheng D, Dietderich D R, English C D, Felice H, Hannaford C R, Prestemon S O, Sabbi G, Scanlan R M, Hikichi Y and Nishioka J 2008 Development of wind-and-react Bi-2212 Accelerator Magnet Technology *IEEE Trans. Appl. Supercond.* **18** 516–9
[19] Shen T, Pei L, Jiang J, Cooley L, Tompkins J, McRae D and Walsh R 2015 High strength kiloampere $Bi_2Sr_2CaCu_2O_x$ cables for high-field magnet applications *Supercond. Sci. Technol.* **28** 065002
[20] Goldacker W, Nast R, Kotzyba G, S I S, Frank A, Ringsdorf B, Schmidt C and Komarek P 2006 High current DyBCO-ROEBEL Assembled Coated Conductor (RACC) *J Phys. Conf. Ser.* **43** 901
[21] Goldacker W, Grilli F, Pardo E, Kario A, Schlachter S I and Vojenčiak M 2014 Roebel cables from REBCO coated conductors: a one-century-old concept for the superconductivity of the future *Supercond. Sci. Technol.* **27** 093001
[22] Takayasu M, Chiesa L, Bromberg L and Minervini J V 2012 HTS twisted stacked-tape cable conductor *Supercond. Sci. Technol.* **25** 014011–21
[23] Takayasu M, Chiesa L, Allen N C and Minervini J V 2016 Present status and recent developments of the twisted stacked-tape cable conductor *IEEE Trans. Appl. Supercond.* **26** 6400210
[24] van der Laan D C, Noyes P, Miller G, Weijers H and Willering G 2013 Characterization of a high-temperature superconducting conductor on round core cables in magnetic fields up to 20 T *Supercond. Sci. Technol.* **26** 045005
[25] Weiss J D, Mulder T, Ten Kate H J J and van der Laan D C 2017 Introduction of CORC® wires: highly flexible, round high-temperature superconducting wires for magnet and power transmission applications *Supercond. Sci. Technol.* **30** 014002
[26] van der Laan D C, Weiss J D and McRae D M 2019 Status of CORC® cables and wires for use in high-field magnets and power systems a decade after their introduction *Supercond. Sci. Technol.* **32** 033001
[27] Weiss J D, van der Laan D C, Hazelton D, Knoll A, Carota G, Abraimov D, Francis A, Small M A, Bradford G and Jaroszynski J 2020 Introduction of the next generation of CORC® wires with engineering current density exceeding 650 Amm^{-2} at 12 T based on SuperPower's ReBCO tapes containing substrates of 25 μm thickness *Supercond. Sci. Technol* **33** 044001
[28] Shen T, Bosque E, Davis D, Jiang J, White M, Zhang K, Higley H, Turqueti M, Huang Y, Miao H and Trociewitz U 2019 Stable, predictable and training-free operation of superconducting Bi-2212 Rutherford cable racetrack coils at the wire current density of 1000 A/mm^2 *Sci. Rep.* **9** 10170
[29] van Nugteren J, Kirby G, Bajas H, Bajko M, Ballarino A, Bottura L, Chiuchiolo A, Contat P-A, Dhallé M, Durante M and Fazilleau P 2018 Powering of an HTS dipole insert-magnet operated standalone in helium gas between 5 and 85 K *Supercond. Sci. Technol.* **31** 065002
[30] Wang X, Dietderich D R, DiMarco J, Ghiorso W B, Gourlay S S A, Higley H C, Lin A, Prestemon S O, van der Laan D C and Weiss J D 2019 A 1.2-T canted cos θ dipole magnet using high-temperature superconducting CORC® wires *Supercond. Sci. Technol.* **32** 075002
[31] van der Laan D C, Weiss J D, Trociewitz U P, Abraimov D, Francis A, Gillman J, Davis D S, Kim Y, Griffin V, Miller G and Weijers H W 2020 A CORC® cable insert solenoid: the first high-temperature superconducting insert magnet tested at currents exceeding 4 kA in 14 T background magnetic field *Supercond. Sci. Technol.* **33** 05LT03
[32] Wang X R *et al* 2020 *Supercond. Sci. Technol.* (to be submitted)
[33] Kreger S T, Gifford D K, Froggatt M E, Soller B J and Wolfe M S 2006 High resolution distributed strain or temperature measurements in single-and multi-mode fiber using swept-wavelength interferometry *Optical Fiber Sensors* OSA Technical Digest (CD) p ThE42
[34] Scurti F, Weiss J D, van der Laan D C and Schwartz J 2020 SMART Conductor on Round Core (CORC®) wire via integrated optical fibers *Supercond. Sci. Technol.* (to be submitted)
[35] Willering G P, van der Laan D C, Weijers H W, Noyes P D, Miller G E and Viouchkov Y 2015 Effect of variations in terminal contact resistances on the current distribution in high-temperature superconducting cables *Supercond. Sci. Technol.* **28** 035001
[36] Michael P C, Bromberg L, van der Laan D C, Noyes P and Weijers H W 2016 Behavior of a high-temperature superconducting conductor on a round core cable at current ramp rates as high as 67.8 kA/s in background fields of up to 19 T *Supercond. Sci. Technol.* **29** 045003